Matched Field Inversion of Geoacoustic Model Parameters using Adaptive Simulated Annealing

by

Colin E. Lindsay
B.Sc., Royal Roads Military College, 1990

A Thesis Submitted in Partial Fulfillment of the
Requirements for the Degree of

MASTER OF SCIENCE

in the Department of Physics and Astronomy

We accept this thesis as conforming to the required standard

[redacted]

Dr. N.R. Chapman, Supervisor (Defence Research Establishment Pacific)

[redacted]

Dr. R.M. Clements, Co-Supervisor (Dept. of Physics and Astronomy)

[redacted]

Dr. L. Kirlin, Outside Member (Dept. of Electrical and Computer Engineering)

[redacted]

Dr. T.S. Hamilton, External Examiner (Geological Survey of Canada)

Supervisor: Dr. N.R. Chapman

ABSTRACT

A method has been developed for the estimation of geoacoustic model parameters by the inversion of acoustic field data using a non-linear optimization procedure based on simulated annealing. The cost function used by the algorithm is the Bartlett matched field processor which relates the measured acoustic field with replica fields calculated by the SAFARI program. Model parameters are perturbed randomly, and the algorithm searches the multidimensional parameter space of geoacoustic models to determine the parameter set corresponding to the best replica field. Convergence is driven by adaptively guiding the search to regions of the parameter space associated with above-average values of the matched field processor. The performance of the method is demonstrated for a vertical line array in a shallow water environment in which the bottom consists of homogeneous elastic solid layers. Simulated data are used to study the effects of uncertainty in the experimental geometry and noise contamination on parameter estimation. Results are presented for the inversion of data obtained in an experiment off the West Coast of Vancouver Island.

Examiners:

[redacted]

Dr. N.R. Chapman, Supervisor (Defence Research Establishment Pacific)

[redacted]

Dr. R.M. Clements, Co-Supervisor (Dept. of Physics and Astronomy)

[redacted]

Dr. L. Kirlin, Outside Member (Dept. of Electrical and Computer Engineering)

[redacted]

Dr. T.S. Hamilton, External Examiner (Geological Survey of Canada)

Contents

List of Figures

List of Tables

Acknowledgments

I'd like to thank my supervisor, Ross Chapman, whose advice proved invaluable. I would also like to thank the National Science and Engineering Research Council, whose scholarship made this work possible, the Canadian Armed Forces, who permitted me to undertake the endeavor, and the department of graduate studies at the University of Victoria, who facilitated my studies.

Chapter 1

Introduction and Overview

Because of the ease with which sound can be transmitted in sea water, acoustic techniques provide a wide range of methods for accumulating knowledge about the environment below the ocean surface. An underwater acoustic source radiates energy as pressure waves. The propagation of these waves depends on the acoustic properties of the sea water and the underlying sediments and rocks. Interaction with the ocean bottom significantly effects the propagation of waterborne acoustic energy. This is especially true in shallow water environments. Sound energy incident on the sea floor is partly transmitted into the bottom. At low frequency, this energy is not rapidly attenuated and may be reflected by sub-bottom reflectors or refracted by positive velocity gradients, thus returning a significant amount of energy to the water column.

The resulting pressure field may be sampled spatially and temporally by a hydrophone array. If the relative geometry between the source and the array is known, the data collected at the array can be used to estimate the geoacoustic properties of the ocean bottom. This is essentially an inverse problem; that is, one can infer the geoacoustic properties of the environment necessary to direct the propagating acoustic waves so as to create the measured pressure field.

The aim of this thesis is to develop a method to estimate the geoacoustic properties of the ocean bottom by inverting acoustic field data. In order to cope with the extreme non-linearity of the inverse problem, the method must be accurate and robust. Accuracy is achieved by modeling the full wave field, and robustness is achieved by using an efficient, adaptive search algorithm. A model with these characteristics is developed in the following chapter, and an overview of the method is presented in the remainder of this chapter.

The first step in developing such an inversion method is to infer a simplified model representation of the environment. The model must describe the depth variation, and possibly range variation, of the following geoacoustic parameters: density, compressional wave velocity and attenuation, shear wave velocity and attenuation. Matched field inversion assesses the accuracy of the model representation by correlating the measured acoustic field with theoretical prediction for the field based on the geoacoustic model.

Traditionally, theoretical acoustic propagation models assume that a source's acoustic field may be represented by plane waves. For many environments, however, the acoustic field is a function of three coordinates: range, depth and bearing. This is the case whenever correlated vertical structures are imposed by bottom interactions in shallow water or upwardly refracting sound-velocity profiles. The inversion method attempts to exploit the complexity of the field by employing accurate theoretical propagation models. The correlation of the replica and measured fields is computed using a matched field beamformer, thereby optimizing signal gain (Fizell, 1987).

The objective of the inversion is to find the replica field that maximizes the output of the matched field beamformer. To do so, replica fields based on several possible geoacoustic models are correlated with the measured field. A search algorithm examines each model and attempts to find the one associated with the highest correlation. This model is the most accurate representation of the geoacoustic properties of the environment.

The search is complicated by the immensity and complexity of the parameter space. Numerous geoacoustic models may cause similar predictions for the acoustic field sampled by a hydrophone array, though they may be physically quite different. The resulting parameter landscape consists of a topography of correlation values that is replete with local optima. Algorithms that search the parameter space by only accepting steps that increase the correlation are prone to converge to one of these locally optimum models. To allow the search to escape from local optima, search methods that accept some steps which decrease the correlation must be employed.

One such method is simulated annealing. Simulated annealing employs statistical mechanics to direct the search. Search steps are performed by randomly perturbing the model parameters. Perturbations that increase the correlation are accepted unconditionally; perturbations that decrease the correlation are accepted with probabilities defined by a Boltzmann distribution. The statistical properties of the Boltzmann distribution must be chosen such that it is appropriate to the topographic variability of the parameter space.

The statistical properties of the Boltzmann distribution are determined by a scaling parameter. The scale parameter must be assigned a value which is low enough that the probability of escaping from highly correlating models is low, but high enough that the probability of escaping from local maxima is high. During the inversion, the scale parameter is gradually reduced. The search therefore accepts fewer perturbations that decrease the correlation, and the decreases it does accept are increasingly smaller. Eventually, the value of the scaling parameter is low enough that the probability of accepting any decrease in correlation approaches zero, and the search converges toward the best parameter configuration in the local vicinity of the parameter space.

Predetermining a reduction schedule for the scale parameter that maintains this balance point is a difficult task, as the significance of a given decrease in correlation is not known *a priori*. The topographic variability of the parameter space is problem specific. Theoretical reduction schedules often give poor results, and a trial and error determination requires prohibitive amounts of computer time. To circumvent the necessity of a predetermined reduction schedule, an algorithm can be employed which assesses the topographic variation of the parameter space during the search. The scale parameter can be adaptively assigned values relative to the average change in correlation per perturbation. *A priori* assumptions about the parameter space may therefore be avoided.

A more general assessment of the topography of the parameter space can be exploited to direct the search toward more promising parameter configurations. The average change in *elevation* (correlation) in each dimension of the parameter space is a measure of the sensitivity of the acoustic field to variations in that parameter. When searching for a *peak* (optimum parameter configuration), it is efficient to preferentially search in directions associated with the greatest change in elevation. Otherwise, time may be wasted circumnavigating peaks, rather than climbing them. Therefore, parameter sensitivity may be used as a guide toward which dimensions warrant greater examination.

With sufficient sampling, the general topography of the parameter space can be assessed. Some regions associated with certain parameter values may be associated with high values of correlation (above sea-level elevation), while regions associated with other parameter values may be associated with low values of correlation (below sea-level). This information can be exploited to preferentially examine parameter configurations in the vicinity of other above-average configurations.

With sufficient generalization, the inversion method developed in this thesis may be applied to any inversion problem. The search algorithm adaptively assesses the landscape of an unknown parameter space and exploits the information acquired to preferentially examine promising regions. The algorithm may therefore be termed an efficient, adaptive search technique. The technique, developed by the author, is herein applied to matched field inversion problems.

The feasibility of the matched field inversion technique is demonstrated by several synthetic inversions in the third chapter. The simulation environment consists of a shallow water column overlying homogeneous elastic solid layers. The field produced by a shallow acoustic source is sampled at a range of 3 km by a vertical array of 10 equally spaced hydrophones. The acoustic field data is inverted for a frequency of 20 Hz.

The first synthetic inversion demonstrates the performance of the algorithm under ideal conditions: a noise-free environment with absolute certainty in the source/array geometry. Then, two examples are presented in order to demonstrate the performance of the method when there is an error in the assumed source/array geometry. This is a common circumstance in most field experiments. Errors in the source range of $^{+1}/_{3}$ and $^{-2}/_{3}$ of a wavelength are considered. Finally, two examples are presented in order to demonstrate the performance of the method when there is noise contamination, a situation arising in all field experiments. Signal-to-noise ratios of 20 dB and 10 dB are considered. Twenty decibels may be considered a realistic noise level for a short range, shallow water experiment. Ten decibels may be considered a high degree of noise contamination.

The applicability of the technique is demonstrated on acoustic field data in the fourth chapter. The data were collected in an experiment conducted by the Defence Research Establishment Pacific, from April 24 to 25, 1985, at a site located on the shelf edge of the Fuca-Tofino Basin off southwestern Vancouver Island. The water was shallow, approximately 200 m deep. The field produced by a shallow acoustic source was sampled at a range of 1.48 km by a vertical array of 10 hydrophones. The hydrophones irregularly spanned the water column, from 82 m to 196 m. The inversion was performed for a frequency of approximately 12 Hz.

The experiment, though not designed for a matched field inversion, was well suited to the task as the source/array geometry was able to be accurately determined, within $\pm^{1}/_{4}$ wavelength, and the signal-to-noise ratio was high, approximately 50 dB.

Conclusions drawn throughout the thesis are presented at the end of the respective chapters. A summary and suggestions for future study are provided in chapter five.

Chapter 2

Matched Field Inversion Method

I. Geoacoustic Model

The determination of geoacoustic models for the ocean bottom is of considerable importance in ocean acoustics. When sound energy interacts with the sea floor, the geoacoustic properties of the bottom must be known in order to model acoustic propagation. An acoustician requires a simplified layered model, as shown in figure 2.1. The model is generally composed of the following parameters:

- Thicknesses of layers, z;
- Compressional wave velocity, C_p, and attenuation, α_p, at the sea floor and as a function of depth;
- Shear wave velocity, C_s, and attenuation, α_s, at the sea floor and as a function of depth; and
- Density, ρ, at the sea floor and as a function of depth.

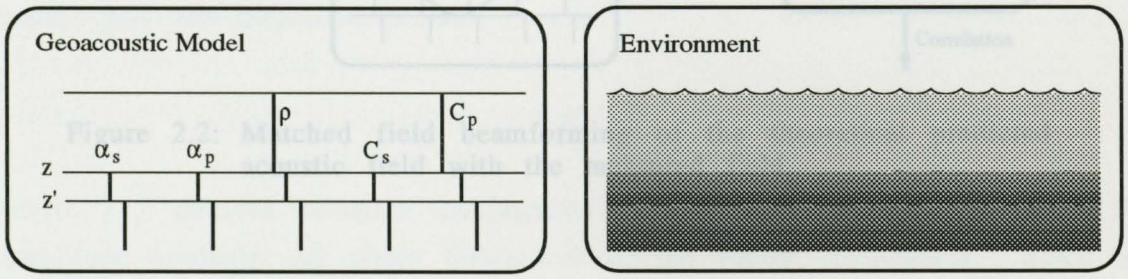

Figure 2.1: Geoacoustic model representation of the ocean environment.

The accuracy of the geoacoustic model may be inferred by correlating acoustic field data with theoretical predictions for the field computed by modeling the acoustic propagation in an environment characterized by the geoacoustic model.

II. Matched Field Beamforming

The correlation of the theoretical acoustic field with the measured field is computed using a field-matching beamformer, as shown in figure 2.2. The beamformer outputs a scalar value for the correlation between zero and one. The value of the correlation indicates how well the replica field matches the measured field. For replica fields computed from a suite of geoacoustic models, the maximum correlation output by the beamformer indicates the geoacoustic model inferred to be the best representation of the environment within the constraints of the model's simplicity and the number of models examined.

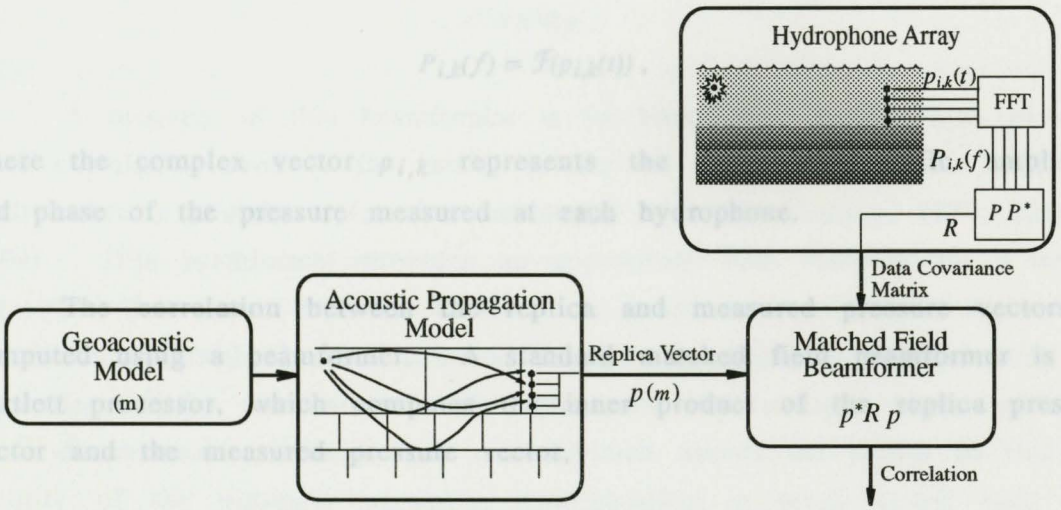

Figure 2.2: Matched field beamforming of the theoretical predicted acoustic field with the measured field.

Accurate acoustic propagation modeling allows an accurate computation of the replica field, and hence a more reliable measure of the validity of the associated geoacoustic model. It is possible to model acoustic propagation exactly using the full-field technique. The technique can be applied if the environment can be represented by a series of horizontally stratified layers.

The solution (Schmidt, 1990) uses a series of integral transforms which reduce the four-dimensional partial differential wave equation to a series of ordinary differential equations in the depth coordinate. These equations are solved numerically for the amplitudes within each layer by matching the interfacial boundary conditions. Inverse integral transforms are used to evaluate the acoustic pressure, p_i, at each hydrophone. For a given model, m, the complex elements of the vector $p(m)$ correspond to the frequency-specific amplitude and phase of the replica pressure field.

The vector of measured pressures, P, is obtained by transforming the received field at the i^{th} hydrophone in the k^{th} time frame, denoted $p_{i,k}(t)$, into the frequency domain using a discrete Fourier transform,

$$P_{i,k}(f) = \mathcal{F}(p_{i,k}(t)) ,$$

where the complex vector $p_{i,k}$ represents the frequency-specific amplitude and phase of the pressure measured at each hydrophone.

The correlation between the replica and measured pressure vectors is computed using a beamformer. A standard matched field beamformer is the Bartlett processor, which computes the inner product of the replica pressure vector and the measured pressure vector,

$$c = p^* P ,$$

where $(^*)$ denotes complex conjugation. The inner product represents the amplitude products and phase differences of the vector components. Since the replica vector is generated with arbitrary phase, it is convenient to evaluate the power of the inner product,

$$C = cc^* = p^* P P^* p .$$

PP^* is generally represented as its covariance matrix, $R = E[PP^*]$, where $E[\cdot]$ is the expectation operator.

Averaging the cross products of the complex data obtained from a sequence of time frames,

$$R_{ij} = \frac{1}{K}\sum_{k=1}^{K} P_{ik}P^{*}_{jk} ,$$

stabilizes the inversion. Here i and j denote the i^{th} and j^{th} hydrophone elements respectively, k denotes the k^{th} time frame, and K is the number of time frames.

The correlation between the replica acoustic field and the measured field may therefore be expressed as

$$C = p^{*}Rp .$$

A property of this beamformer is its broad main lobe, which provides good correlation even if the model is not in excellent agreement with the environment, a situation referred to as model mismatch [Tolstoy, 1989; Gingras, 1989]. This beamformer provides an appropriate cost function for a search algorithm that must examine a suite of geoacoustic models. Reasonable correlation is obtained when examined models are close to approximating the properties of the environment. For problems with a large parameter space (multi-dimensional problems), this cost function allows the search to find the vicinity of the optimum parameter configuration, a much easier task than finding the optimum configuration itself.

III. Matched Field Optimization

A search algorithm attempts to find the optimum value of a function of many variables. The value of this cost function is a measure of the *goodness-of-fit* of a representation of a complex system. The value depends on the configuration of the many system components. The optimization of the function is therefore commonly referred to as combinatorial optimization.

In matched field optimization, the cost function is the matched field beamformer, which provides a quantitative measure of the accuracy of the model representation of the ocean bottom. The beamformer output depends on the configuration of the model parameters.

The parameter space for combinatorial optimization problems is discrete, but factorially large, and cannot, in practice, be thoroughly explored. All exact methods known for determining the optimum value in the parameter space require a computing effort that increases exponentially with the number of parameters. As such, heuristic solution techniques are often employed. The most common technique is iterative improvement. One begins with an initial parameter configuration, and a standard perturbation operation is applied to each parameter until a new configuration is found that improves the value of the cost function. The new configuration is adopted and the process continued until no further improvement can be found.

Iterative improvement consists of a search through the parameter space for reconfigurations that increase the value of the cost function. Search methods employing such deterministic transition rules are prone to trapping by local maxima (parameter configurations with a higher value of the cost function than adjacent configurations, but less than other, distant configurations). In order to find the optimum configuration, the search must begin in the vicinity of the search space closer to the global optimum than any local maxima. For realistic problems, such confidence in the initial configuration is unrealistic. If only modest *a priori* knowledge about the environment is available, such stringent initial conditions cannot be imposed.

In order to avoid trapping by local maxima, iterative improvement must be generalized to accept parameter reconfigurations that decrease the value of the cost function. The frequency of acceptance of such reconfigurations may be controlled by assigning a probability of acceptance proportional to the decrease in correlation. Simulated annealing is a technique that employs such probabilistic transition operators (Kirkpatrick *et. al.*, 1983; Kirkpatrick, 1984; van Laarhoven and Arts; 1987).

A. Simulated Annealing

Simulated annealing is based on an analogy with the thermodynamic process by which liquids cool and form crystals. Simulated annealing employs statistical mechanics to describe the average behavior of a physical system in thermal equilibrium. The Boltzmann probability distribution,

$$P(\boldsymbol{r}) \sim \exp(-E(\boldsymbol{r})/T),$$

expresses the idea that a system in thermal equilibrium at temperature T has its energy, E, probabilistically distributed over all possible configurations $\boldsymbol{r}$. Thermal agitation perturbs the system continuously. Perturbations that increase system energy are allowed, although they are less probable than those which decrease it. As the temperature decreases, the Boltzmann distribution assigns progressively greater probability to low-energy configurations. In the limit as $T \rightarrow 0$, the Boltzmann distribution collapses to the ground state for the system. This ground state corresponds to a pure crystal which represents the global minimum energy configuration for the system.

In matched field optimization using simulated annealing, illustrated in figure 2.3, the geoacoustic model is analogous to a system of particles. Thermal agitation is applied to the system by a perturbation operator which selects a new parameter configuration. The allowed values that a perturbed parameter may assume correspond to the allowed energy states of its associated particle. The resultant change in correlation (analogous to the system energy) is assessed. If the correlation has been increased, the perturbation is accepted unconditionally; if the correlation has been decreased, the perturbation is accepted probabilistically. If the perturbation is accepted, the new parameter configuration is adopted, and the process repeated. The probability of accepting perturbations that decrease the correlation is gradually reduced until no further improvement can be found, at which point the model parameters freeze into an optimum configuration.

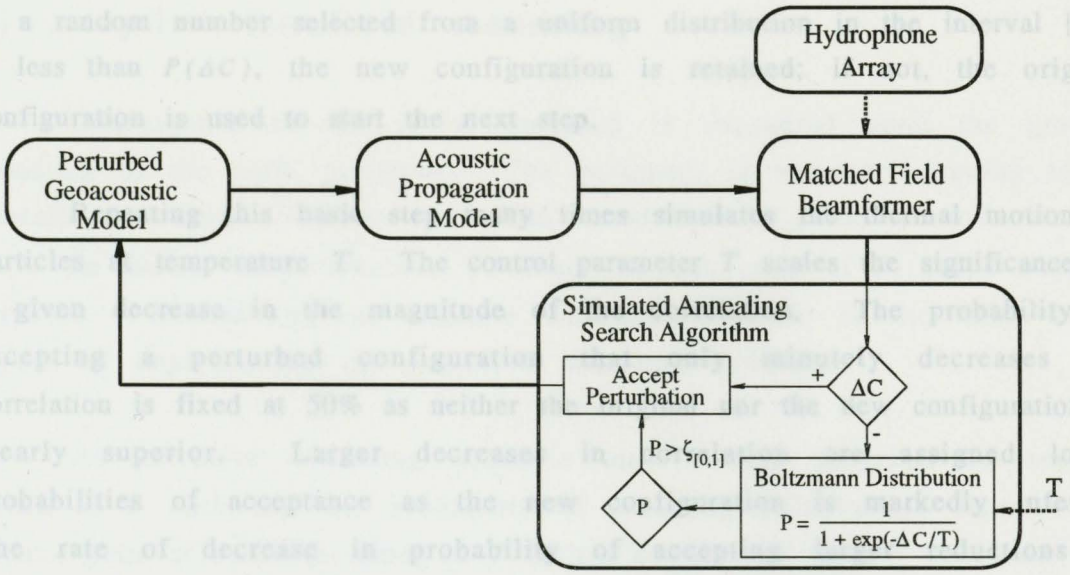

Figure 2.3: Matched field optimization using simulated annealing.

Model perturbations are performed by setting a parameter to a new value within its assigned range,

$$X = x_{min} + \zeta(x_{max} - x_{min}) ,$$

where x_{max} and x_{min} represent the upper and lower bounds on the range respectively, and ζ is a random number generated over the range [0,1]. By selecting parameter values from a uniform probability distribution, the entire parameter space is evenly sampled. The search is therefore less prone to trapping by local maxima than techniques that perturb a parameter as a function of its previous value.

If the perturbed model increases the correlation, the parameter configuration is retained. If the perturbed model decreases the correlation by ΔC, the probability of acceptance is taken to be

$$P(\Delta C) = \frac{1}{1 + \exp(-\Delta C/T)} .$$

If a random number selected from a uniform distribution in the interval [0,1] is less than $P(\Delta C)$, the new configuration is retained; if not, the original configuration is used to start the next step.

Repeating this basic step many times simulates the thermal motion of particles at temperature T. The control parameter T scales the significance of a given decrease in the magnitude of the correlation. The probability of accepting a perturbed configuration that only minutely decreases the correlation is fixed at 50% as neither the original nor the new configuration is clearly superior. Larger decreases in correlation are assigned lower probabilities of acceptance as the new configuration is markedly inferior. The rate of decrease in probability of accepting larger reductions in correlation is determined by assigning a fixed probability of accepting an average magnitude decrease in correlation. A curve of probabilities, as shown in figure 2.4, is fit through these two points, and the probability of accepting any magnitude decrease in correlation may be extrapolated.

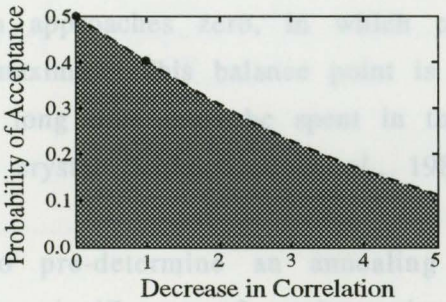

Figure 2.4: Probability of accepting a perturbation associated with a given decrease in correlation (in units of an average magnitude change in correlation, $|\Delta C|_{avg}$).

During the inversion, the value of T is gradually reduced so that the probability of accepting model reconfigurations that decrease the correlation also decreases. At low enough values of T, reconfigurations that decrease the correlation are no longer accepted. If the search space has been evenly sampled and the parameter T reduced slowly and judiciously, the model parameters freeze into the global optimum configuration.

B. Adaptive Simulated Annealing

Convergence to the global optimum is dependent upon the gradual reduction of the scale parameter. The parameter is reduced according to an annealing schedule. This consists of an initial value, T_O, the rate of reduction of T, the number of perturbations performed at each value of T, and a stopping criterion. Determining an effective annealing schedule is the most subtle aspect of implementing the simulated annealing technique.

An effective annealing schedule must assign progressively smaller values of T such that the probability of accepting perturbations represents a balance point at which the value of T is low enough that models associated with high values of correlation are preferred, but high enough for the search to accept transitions between such models. If the value of T is too high, the probability of accepting significant decreases in correlation approaches 50%, in which case the search becomes a random walk through the parameter space. If the value of T is too low, the probability of accepting even slight reductions in correlation approaches zero, in which case the search loses the ability to escape local maxima. This balance point is analogous to the freezing point of the liquid. A long time must be spent in the vicinity of the freezing point to produce a pure crystal (Kirkpatrick *et. al.*, 1983).

It is difficult to pre-determine an annealing schedule that maintains this balance point as the significance of a given change in correlation, ΔC, is not known *a priori*. Theoretical annealing schedules often give poor results, and trial and error determination requires prohibitive amounts of computer time (Basu and Fraser, 1990). This difficulty can be overcome by monitoring the average change in correlation per perturbation during the inversion, as shown in figure 2.5. By fixing the probability, P, of accepting an average magnitude decrease in correlation, $|\overline{\Delta C}|$,

$$P = \frac{1}{1 + \exp(-|\overline{\Delta C}|/T)},$$

appropriate values of T may be assigned,

$$T = \frac{|\overline{\Delta C}|}{-\ln\left(\frac{1}{P} - 1\right)}.$$

Incorporating a feedback loop to determine the appropriate value of the scale parameter ensures realistic acceptance probabilities,

$$P(\Delta C) = \frac{1}{1 + \exp\left(-\ln\left(\frac{1}{P} - 1\right)\frac{\Delta C}{|\overline{\Delta C}|}\right)}.$$

Thus, the need for a pre-determined reduction schedule for the control parameter is eliminated.

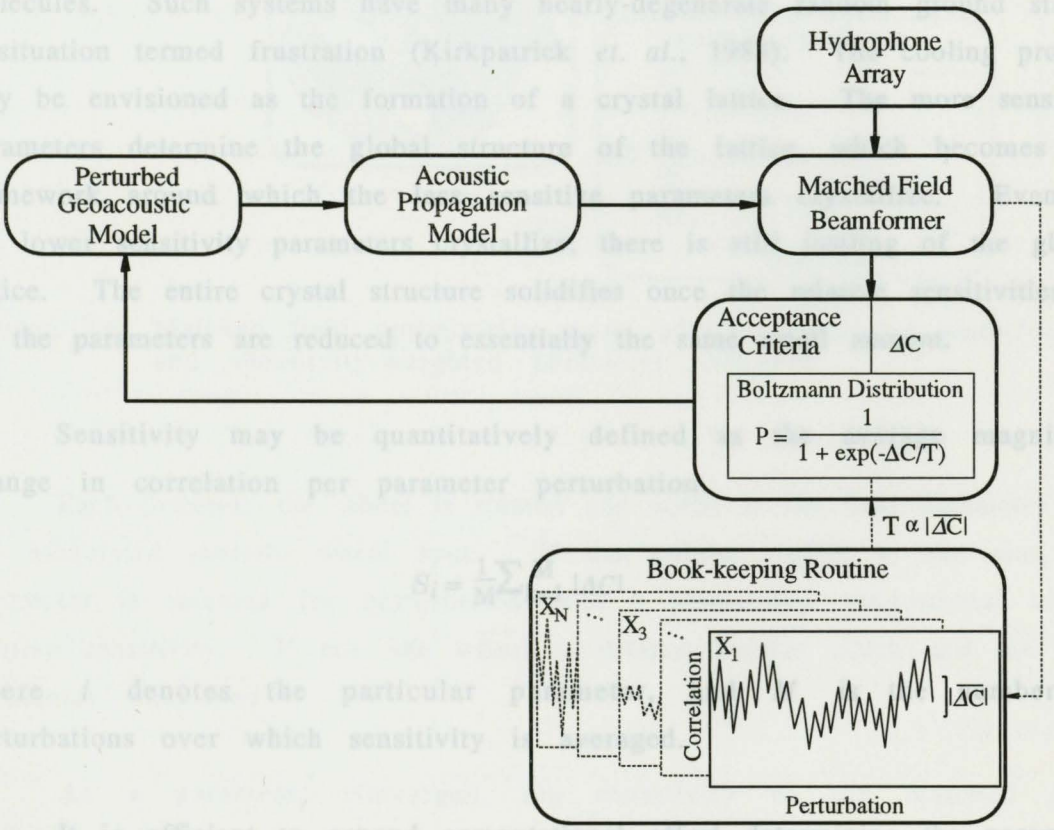

Figure 2.5: Matched field optimization using adaptive simulated annealing.

C. Parameter Sensitivity

As stated earlier, simulated annealing is based on an analogy with the cooling of a homogeneous liquid, in which all the particles are alike and the ground state is a regular crystal. However, realistic systems are generally not composed of parameters that have equal effects in determining the value of the cost function. This is the case in a matched field inversion problem. Perturbations of parameters to which the acoustic field is highly sensitive are associated with large changes in correlation; parameters to which the acoustic field is relatively insensitive cause only slight changes.

Optimizing a system of parameters with disparate sensitivities is analogous to cooling a heterogeneous liquid composed of several different molecules. Such systems have many nearly-degenerate random ground states, a situation termed frustration (Kirkpatrick *et. al.*, 1983). The cooling process may be envisioned as the formation of a crystal lattice. The more sensitive parameters determine the global structure of the lattice, which becomes the framework around which the less sensitive parameters crystallize. Even as the lower sensitivity parameters crystallize, there is still jostling of the global lattice. The entire crystal structure solidifies once the relative sensitivities of all the parameters are reduced to essentially the same small amount.

Sensitivity may be quantitatively defined as the average magnitude change in correlation per parameter perturbation,

$$S_i = \frac{1}{M} \sum_{k=1}^{M} |\Delta C| ,$$

where i denotes the particular parameter, and M is the number of perturbations over which sensitivity is averaged.

It is efficient to expend computational effort determining the parameter values in proportion to their relative sensitivity. Computational effort may be allocated between parameters by the frequency of selection for perturbation.

Implementing sensitivity-weighted parameter selection is analogous to a notched wheel, upon which each parameter has a roulette wheel with a slot sized in proportion to its relative sensitivity, as shown in figure 2.6.

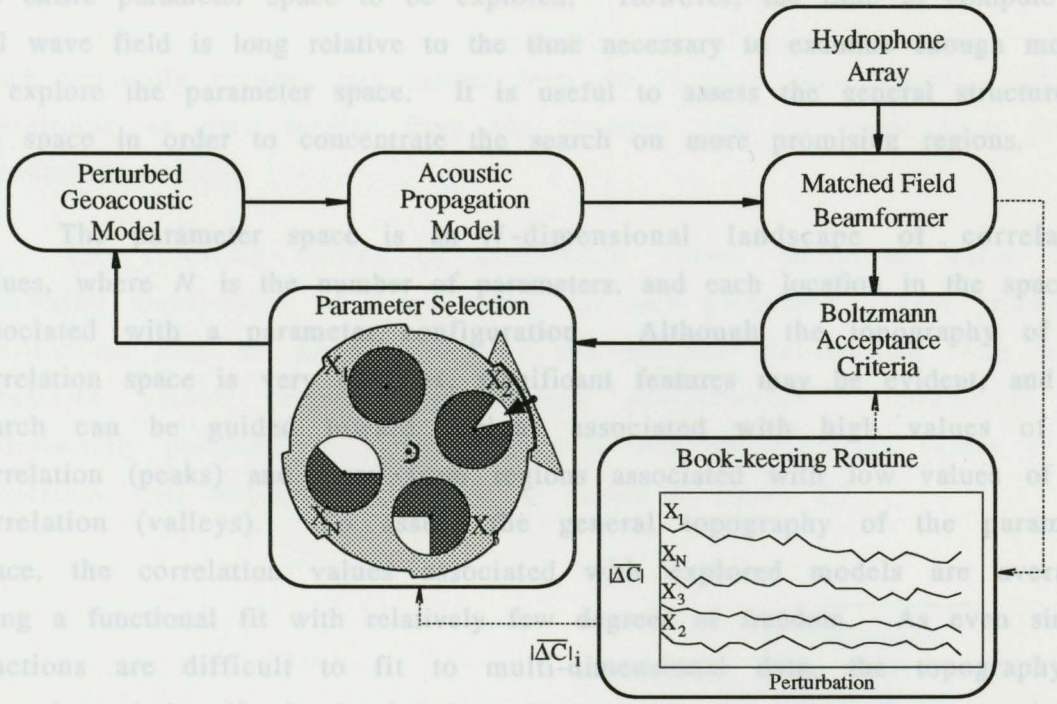

Figure 2.6: Matched field optimization using adaptive simulated annealing and sensitivity-weighted parameter selection.

Each iteration, the wheel is rotated one notch to the next parameter and the associated roulette wheel spun. If the pointer points to the slot, the parameter is selected for perturbation with a probability proportional to its relative sensitivity. If not, the wheel is rotated another notch and the next parameter examined.

As a parameter converges, the sensitivity of the matched field beamformer to perturbations in that parameter decreases. As the more sensitive parameters converge, the search expends more computational resources in determining the values of parameters with lower sensitivities.

D. Self-Guided Simulated Annealing

Conventional simulated annealing is an efficient point-to-point search technique, which is effective if the time for each iteration is short enough for the entire parameter space to be explored. However, the time to compute the full wave field is long relative to the time necessary to examine enough models to explore the parameter space. It is useful to assess the general structure of the space in order to concentrate the search on more promising regions.

The parameter space is an N-dimensional landscape of correlation values, where N is the number of parameters, and each location in the space is associated with a parameter configuration. Although the topography of the correlation space is very complex, significant features may be evident, and the search can be guided toward regions associated with high values of the correlation (peaks) and away from regions associated with low values of the correlation (valleys). To assess the general topography of the parameter space, the correlation values associated with explored models are averaged using a functional fit with relatively few degrees of freedom. As even simple functions are difficult to fit to multi-dimensional data, the topography is approximated by N simple functions representing the averaged topography in each dimension. There is scatter about the functions resulting from the fact that different models sharing similar values of a parameter are associated with different values of correlation. If the scatter may be assumed to be a random variate, it may be smoothed out by fitting functions to the data subject to the constraint that they minimize the scatter about the functions.

The data consist of discrete points, (x,c). The independent variable, x, represents the value of a particular parameter, and the dependent variable c, represents the correlation. Given a functional form, $f(x)$, a fitting routine determines the values of the coefficients such that the *distance* of the data from the function,

$$\sum_{r=1}^{m} |c_r - f(x_r)| ,$$

is a minimum. It is appropriate to minimize this norm as opposed to the more conventional least-squares norm,

$$\sum_{r=1}^{m}(c_r - f(x_r))^2 ,$$

which implicitly weights data further from the function more heavily. This is undesirable as data further from the function tend to result from poorly correlating models.

The resulting curves of correlation versus parameter value form probability distributions of *good* values for each parameter. These probability distributions may be used to replace the uniform distributions from which parameter values are selected during perturbation. Parameters are preferentially perturbed to values associated with above-average values of the correlation, thus directing the search, as shown in figure 2.7.

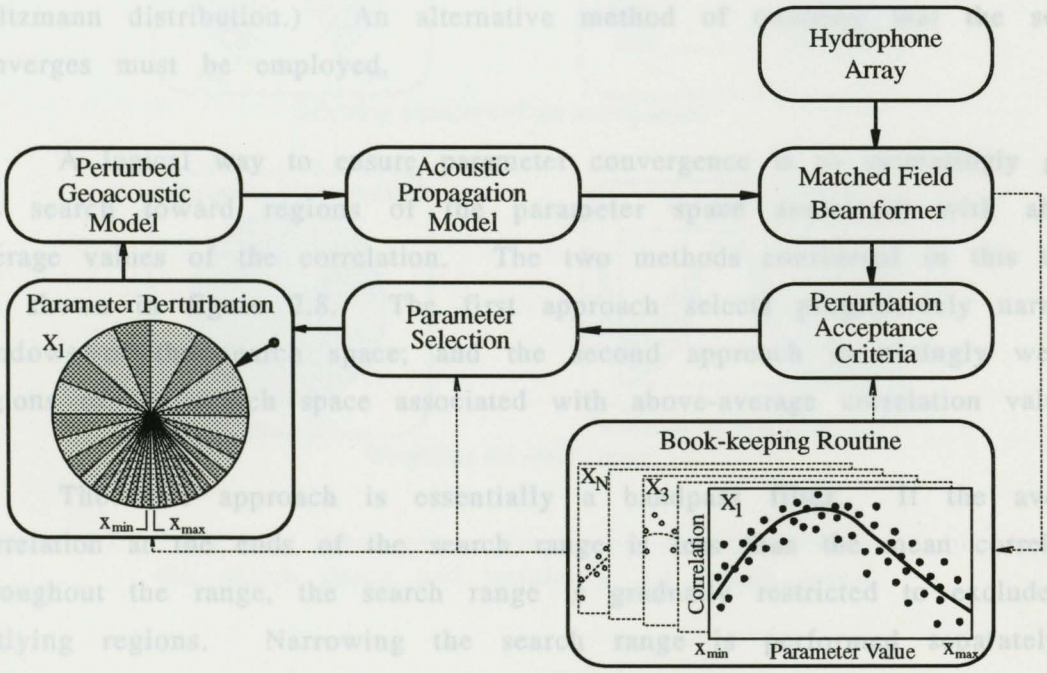

Figure 2.7: Matched field optimization using adaptive simulated annealing, weighted parameter selection and perturbation.

Parameter perturbation may be envisioned as the spinning of a roulette wheel on which each slot corresponds to a parameter value, and the width of the slot corresponds to the average correlation (from the fitted curve) associated with that value. Parameter values associated with high values of correlation have wider slots, and hence a greater probability of selection. The generalization to a continuous spectrum of parameter values is trivial.

E. Parameter Convergence

Conventional simulated annealing converges toward a solution by gradually reducing the scaling parameter such that the probability of accepting perturbations that decrease the correlation gradually decreases. Eventually, no perturbations are accepted and the search freezes at the latest model configuration. In removing the problematic reduction schedule for the scaling parameter, the principal method of ensuring convergence has also been removed. (Convergence is also weakly driven by the form of the Boltzmann distribution.) An alternative method of ensuring that the search converges must be employed.

A logical way to ensure parameter convergence is to increasingly guide the search toward regions of the parameter space associated with above-average values of the correlation. The two methods considered in this thesis are shown in figure 2.8. The first approach selects progressively narrower windows of the search space; and the second approach increasingly weights regions of the search space associated with above-average correlation values.

The first approach is essentially a bandpass filter. If the average correlation at the ends of the search range is less than the mean correlation throughout the range, the search range is gradually restricted to exclude the outlying regions. Narrowing the search range is performed separately in each dimension, in proportion to the difference between the mean correlation and the average correlation at each end of the parameter search range. The

algorithm can be designed to restrict the search space so as to yield a reasonable solution within a prescribed number of iterations.

The second approach involves weighting the probability distributions of correlation value versus parameter value, such that there is an increasing probability of selecting parameter values associated with above-average values of the correlation. The algorithm can also be designed to restrict the search space, as it suppresses parameter perturbations to values associated with poor values of the correlation, so as to yield a reasonable solution within a prescribed number of iterations. This approach has an advantage in that it doesn't assume that poorly correlating models occur in the outlying regions of the search space.

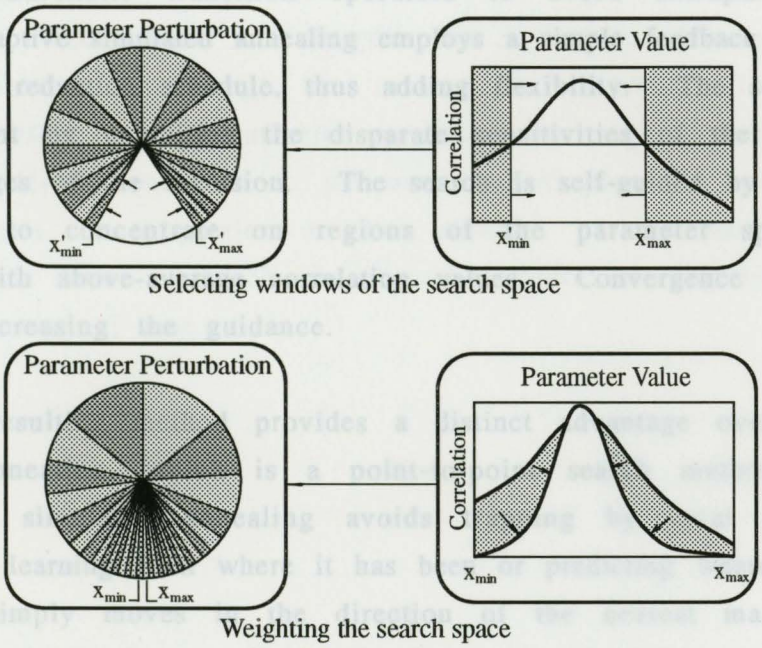

Figure 2.8: Parameter convergence driven by selecting windows of the search space and weighting the search space.

Both approaches have the advantage over arbitrarily reducing the scale parameter, in that convergence is only driven in proportion to the strength of

the correlation trends apparent in the data. If such trends are weak, the algorithm will converge slowly. If such trends are strong, the algorithm will converge quickly.

IV. Summary

Implementing matched field inversion is relatively straightforward. The structure of a geoacoustic model representation of the ocean bottom is inferred, and a suite of models are used to compute replica fields that are correlated with a measured field by a matched field beamformer. An optimization algorithm is used to search the parameter space for the best model. Distinct from conventional optimization methods, simulated annealing employs probabilistic transition operators to avoid entrapment by local optima. Adaptive simulated annealing employs a simple feedback loop in place of the rigid reduction schedule, thus adding flexibility. The search is made more efficient by exploiting the disparate sensitivities of the parameters at different stages of the inversion. The search is self-guided by using historic information to concentrate on regions of the parameter space that are associated with above-average correlation values. Convergence is ensured by gradually increasing the guidance.

The resulting method provides a distinct advantage over conventional simulated annealing, which is a point-to-point search method. Although conventional simulated annealing avoids trapping by local optima, it is incapable of learning from where it has been or predicting where it should go next. It simply moves in the direction of the nearest maxima with an occasional downhill foray. If the landscape is not stationary, but rather is evolving with time, the search will be frustrated unless the solution is stochastically stationary. If the solution is also migrating in the parameter space, conventional simulated annealing may fail entirely, especially if the solution migrates faster than the search is able to circumnavigate local optima.

In contrast, adaptive simulated annealing assesses the landscape as it searches, and is therefore able to infer general trends in correlation, if any exist. Experience has shown that if these trends are not present, a search is largely futile in any event. If the landscape is evolving with time, random fluctuations will be damped out in the same manner in which the trends are identified. If the solution is migrating through the parameter space, the progressive assessment of the landscape will account for these changes in the general trends. As well, as the search is not point-to-point, the search need not follow the solution through the space. As such, the algorithm developed in this chapter is appropriate for real time, evolving inversion problems.

The method is independent of the initial parameter configuration, and is straightforward to generalize to any combinatorial optimization problem. The control parameters are problem aspecific, as they are chosen by statistical consideration. The method can therefore be applied to different and/or more complex problems. Although the assumptions on which it operates are increasingly valid in low-dimension problems, or high dimension problems with a considerable variation in parameter sensitivities, the search algorithm only converges in proportion to the strength of the correlation trends apparent in the data. As such, the algorithm infers the best solution possible in a given amount of time.

Chapter 3

Simulation Study

This chapter presents several inversions of a synthetic environment in order to demonstrate the feasibility of the method developed in the previous chapter. The first inversion is performed under optimum conditions: a noise-free environment and absolute certainty in the source/array geometry. Next, two examples are presented in order to demonstrate the effect of an error in the assumed source/array geometry. Errors in the source position of $+1/3$ and $-2/3$ of a wavelength are considered. Finally, two examples are presented in order to demonstrate the effects of noise contamination of the measured pressures. Realistic and high noise levels are considered, represented by signal-to-noise ratios of 20 dB and 10 dB respectively.

I. Geoacoustic Environment

The synthetic environment is shown in figure 3.1. It has three layers: a water layer of constant thickness and velocity, acting as a wave guide, overlying a homogeneous elastic layer of unconsolidated sediment resting on a half space whose properties resemble sedimentary rock.

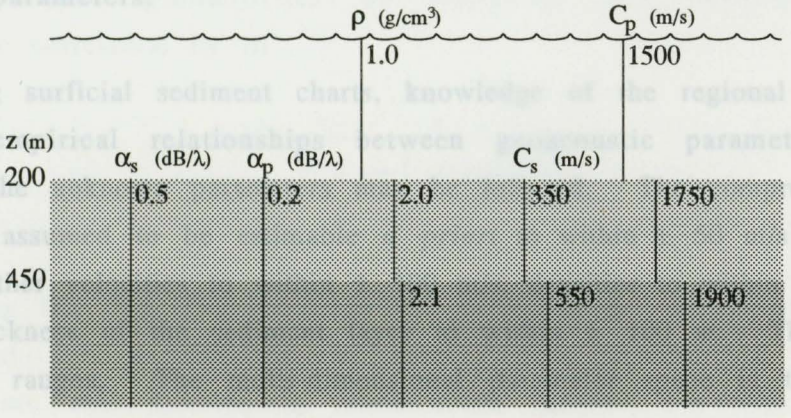

Figure 3.1: Geoacoustic properties of the simulation environment.

The water column is 200 m deep, the sediment layer is 250 m thick, and the underlying sedimentary bedrock is treated as a half space. The compressional velocity is C_p = 1500 m/s in the water, C_p' = 1750 m/s in the sediment, and C_p'' = 1900 m/s in the bedrock. The shear velocity is C_s = 350 m/s in the sediment, and C_s' = 550 m/s in the bedrock. The density is ρ = 1.0 g/cm^3 in the water, ρ' = 2.0 g/cm^3 in the sediment, and ρ'' = 2.1 g/cm^3 in the bedrock. The compressional wave attenuation is α_p = 0.2 dB/λ, and the shear wave attenuation is α_s = 0.5 dB/λ throughout the bottom.

The acoustic field generated by a shallow acoustic source, at 20 m depth, is sampled by a vertical array of 10 equally spaced hydrophones spanning the lower half of the water column, 3 km distant. The ratio of the water depth to the range is quite small, indicating significant bottom-interaction. The inversion is performed at a frequency of 20 Hz.

II. The Inversion Algorithm

The objective of the inversion algorithm is to estimate the geoacoustic properties of the synthetic ocean bottom, with the exception of the attenuation of compressional and shear waves, which were fixed at reasonable values (Hamilton, 1987). The parameter search space of geoacoustic models is defined as the continuum in seven dimensions bound by the permissible ranges of the unknown parameters.

Using surficial sediment charts, knowledge of the regional geology and published empirical relationships between geoacoustic parameters, realistic ranges on the unknown parameters may be inferred. The compressional wave velocity is assumed to be estimable *a priori* to within ± 50 m/s of the actual value, all other velocities to within ± 100 m/s, densities to within ± 0.1 g/cm^3, and the thickness of the sediment layer to within ± 100 m. These represent fairly wide ranges. The multi-dimensional parameter space is therefore very large.

The inversion is initialized with a geoacoustic model composed of parameters assigned random values from within these ranges. The model is then iteratively perturbed by reassigning individual parameters random values from within their respective ranges.

For each perturbed model, a theoretical prediction of the acoustic field is computed using the fast field solution calculated by the SAFARI program (Schmidt, 1990). The time for the computation of each replica field is approximately 1.5 s on a VAX 9000. Each replica field is correlated with the measured acoustic field, itself synthetically generated using the SAFARI program. The correlation is computed using a Bartlett beamformer.

Parameter reconfigurations that increase the correlation are accepted unconditionally. Perturbations that decrease the correlation are accepted with probabilities assigned by a Boltzmann probability distribution. The probability of accepting such perturbations decreases exponentially with the magnitude of the decrease in correlation. The rate of the exponential decrease is fixed by assigning a 40% probability of accepting an average magnitude decrease in correlation, $|\overline{\Delta C}|$. The scale parameter is therefore set to

$$T = \frac{|\overline{\Delta C}|}{-\ln\left(\frac{1}{0.4} - 1\right)},$$

ensuring realistic probabilities of accepting any perturbation which decreases the correlation by ΔC,

$$P(\Delta C) = \frac{1}{1 + \exp\left(-.405465 \frac{\Delta C}{|\overline{\Delta C}|}\right)}.$$

During the first 350 iterations (50 iterations per parameter), parameters are selected for perturbation in round robin fashion. Subsequently, parameters are still selected in round robin fashion, but with probabilities

proportional to their relative sensitivities. Sensitivities are computed using the moving average over the 50 most recent perturbations of each parameter.

The correlation values associated with individual parameter values from each explored model are averaged to form probability distributions of correlation values associated with each parameter. The correlation versus parameter value data were averaged by fitting a fourth-order polynomial. The low order of the polynomial maximizes the data smoothing while having enough degrees of freedom to represent one peak (a cluster of high correlation values assumed to correspond to the best parameter value), and two troughs (clusters of low correlation values assumed to correspond to poor parameter values).

The search space is progressively windowed to exclude regions associated with below-average correlation values using the method described in the previous chapter. The search space is restricted in each dimension in proportion to parameter sensitivity and the significance of the correlation trends in that dimension. The significance of the correlation trends is taken as the difference between the average correlation at the ends of the parameter range and the average over the range. Windowing of the search space occurs every time a threshold of 300 distinct values of the most sensitive parameter is crossed. The total restriction of the search space is 1% each time,

$$\Delta X_i = \frac{S_i}{\Sigma_N S} \cdot \frac{C_{avg} - C_{end}}{\Sigma_N (C_{avg} - C_{end})} \cdot 0.01 \cdot (x_{max} - x_{min})_i .$$

More sensitive parameters, and those parameters that display more significant clustering of high correlation values converge more rapidly. This scheme ensures a significant reduction in the size of the search space over the number of iterations chosen, 20000.

To reduce the computational overhead caused by storing and retrieving each model examined, models containing parameter values outside the restricted search window are dropped from the data pool.

III. Simulation Results

A. Optimum conditions

The performance of the inversion algorithm under optimum conditions is presented in figures 3.2-3.4. Figure 3.2, a plot of correlation versus iteration illustrates the convergence properties of the search.

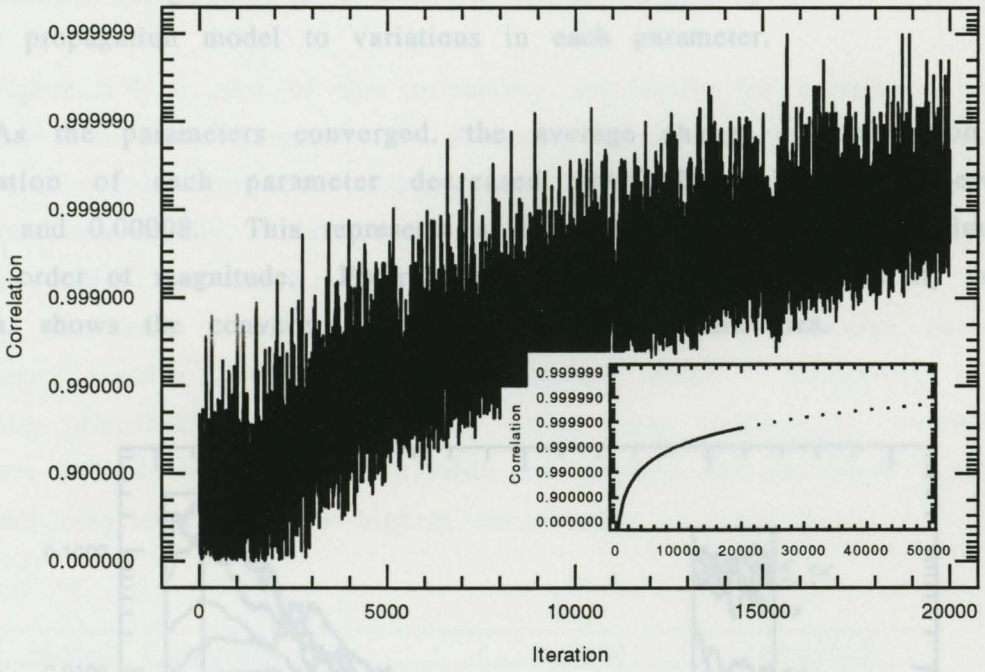

Figure 3.2: Correlation versus iteration for a synthetic inversion under optimum conditions.

Although the correlation values of successively examined models varied considerably, the average correlation increased steadily. The average correlation increased over four orders of magnitude, and converged to approximately 0.9999 by iteration 20000. This represents a near-exact replication of the acoustic field. The accuracy of the replication appears to be asymptotically approaching the machine tolerance, 10^{-6}, as shown by the inset in figure 3.2, a logarithmic fit to the correlation values using the l_1 norm.

The correlation output by the matched field processor was most sensitive to perturbations of the sediment layer thickness and the compressional wave velocities, less so to perturbations of the shear wave velocity and density in the sediment, and least sensitive to perturbations of the shear wave velocity and density in the bedrock. Perturbing the most sensitive parameter caused an average change in correlation of approximately 0.2. In contrast, perturbing the least sensitive parameter caused an average change in correlation of approximately 0.0025. The difference in sensitivity of almost two orders of magnitude is a function of the sensitivity of the theoretical acoustic propagation model to variations in each parameter.

As the parameters converged, the average change in correlation per perturbation of each parameter decreased until they all varied between 0.00002 and 0.00008. This represents a difference in sensitivity approximately half an order of magnitude. Figure 3.3, a plot of parameter sensitivity versus iteration, shows the convergence of the parameter sensitivities.

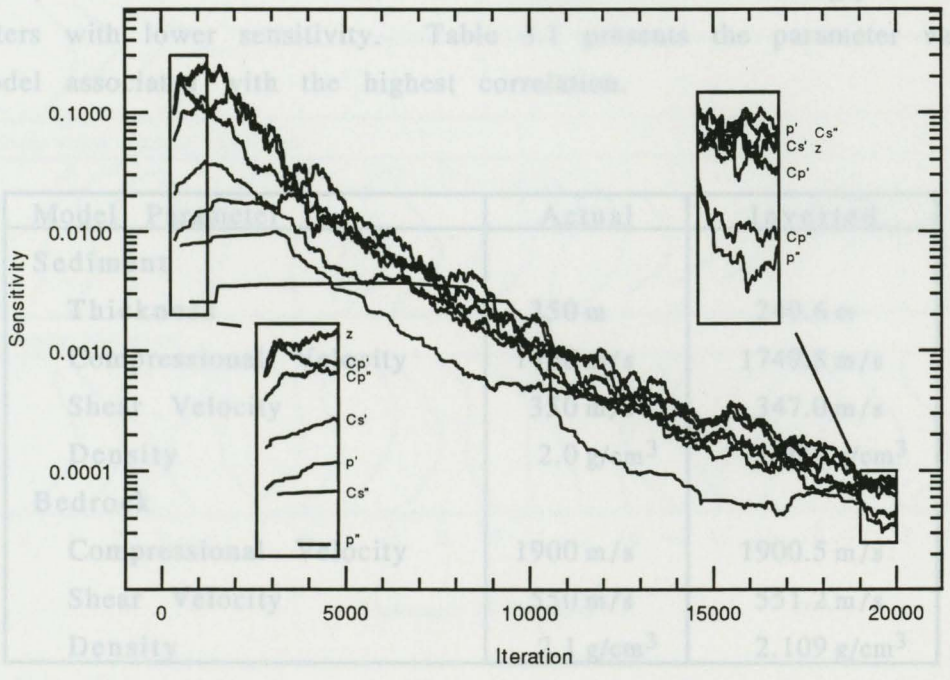

Figure 3.3: Parameter sensitivity versus iteration for a synthetic inversion under optimum conditions.

During the inversion, parameter sensitivity decreased steadily. This is to be expected as the range of values a parameter may assume determines the sensitivity of the matched field processor to variations in that parameter. If a parameter can assume vastly different values, the associated acoustic fields will be quite different and the output of the matched field processor will vary greatly. If a parameter can only assume a narrow range of values, the acoustic field will be essentially the same and the output of the matched field processor will similarly vary only slightly. The restriction of the parameter ranges during convergence caused the decrease in sensitivity.

Figure 3.4, a plot of the probability distribution of correlation values associated with each parameter in thousand iteration increments, illustrates the results of the parameter convergence. The most sensitive parameters converged most rapidly. The moderately sensitive parameters did not begin to converge until the more sensitive parameters were essentially fixed. Similarly, the least sensitive parameters did not begin to converge until the moderately sensitive parameters were essentially fixed. Variability in the probability distributions of correlation values was increasingly evident in parameters with lower sensitivity. Table 3.1 presents the parameter values of the model associated with the highest correlation.

Model Parameter	Actual	Inverted
Sediment		
Thickness	250 m	249.6 m
Compressional Velocity	1750 m/s	1749.8 m/s
Shear Velocity	350 m/s	347.0 m/s
Density	2.0 g/cm^3	1.987 g/cm^3
Bedrock		
Compressional Velocity	1900 m/s	1900.5 m/s
Shear Velocity	550 m/s	551.2 m/s
Density	2.1 g/cm^3	2.109 g/cm^3

Table 3.1: Parameter values of the geoacoustic model associated with the highest correlation.

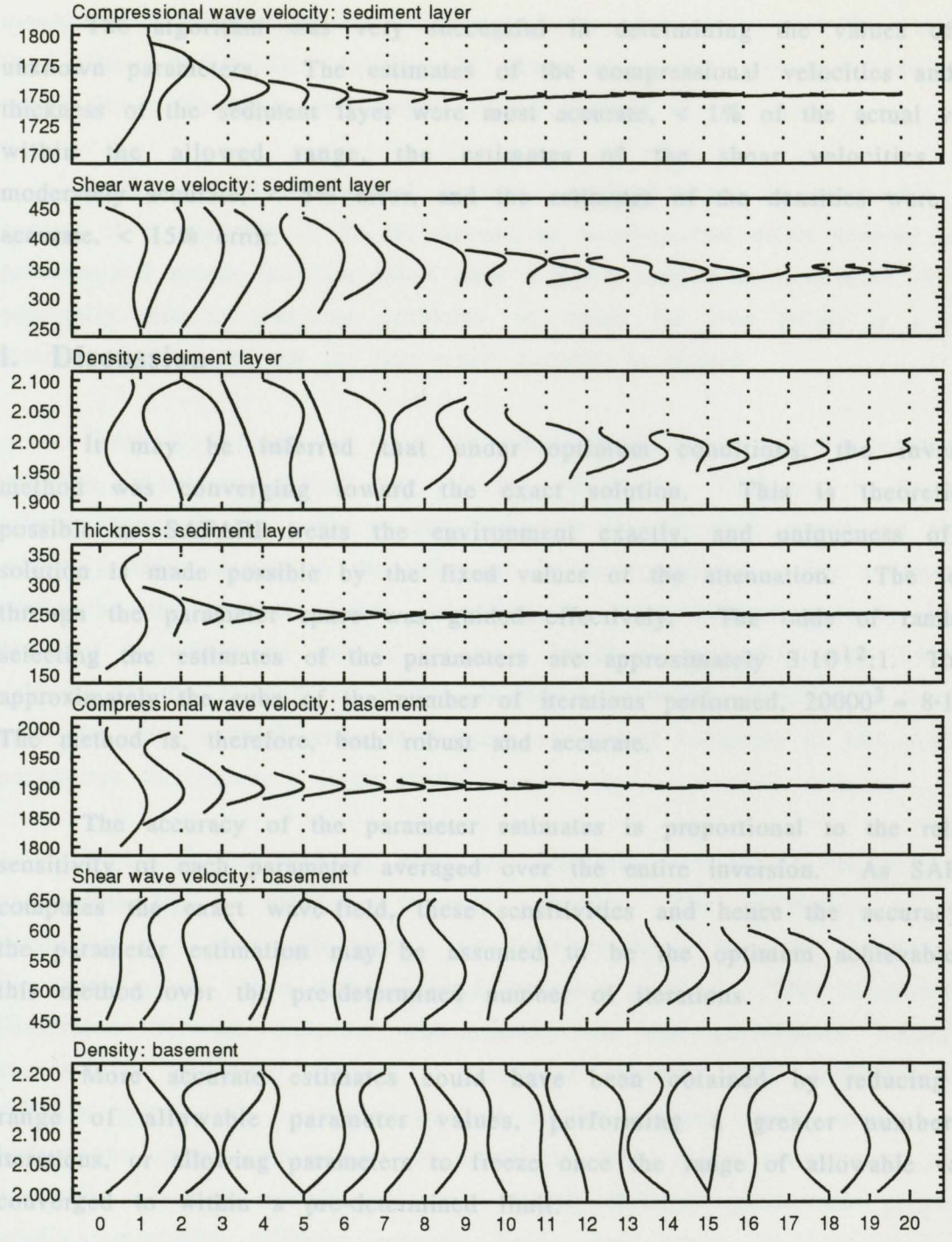

Figure 3.4: Convergence in geoacoustic parameter values with iteration. The curves are probability distributions determined by averaging the correlation associated with parameter values over several models.

The algorithm was very successful in determining the values of the unknown parameters. The estimates of the compressional velocities and the thickness of the sediment layer were most accurate, < 1% of the actual values within the allowed range, the estimates of the shear velocities were moderately accurate, < 5% error, and the estimates of the densities were least accurate, < 15% error.

i. Discussion

It may be inferred that under optimum conditions, the inversion method was converging toward the exact solution. This is theoretically possible as SAFARI treats the environment exactly, and uniqueness of the solution is made possible by the fixed values of the attenuation. The search through the parameter space was guided effectively. The odds of randomly selecting the estimates of the parameters are approximately $3 \cdot 10^{12}$:1. This is approximately the cube of the number of iterations performed, $20000^3 \approx 8 \cdot 10^{12}$. The method is, therefore, both robust and accurate.

The accuracy of the parameter estimates is proportional to the relative sensitivity of each parameter averaged over the entire inversion. As SAFARI computes the exact wave-field, these sensitivities and hence the accuracy of the parameter estimation may be assumed to be the optimum achievable by this method over the pre-determined number of iterations.

More accurate estimates could have been obtained by reducing the range of allowable parameter values, performing a greater number of iterations, or allowing parameters to freeze once the range of allowable values converged to within a pre-determined limit.

Narrowing the initial range of allowable parameter values may not be reasonable. The range should be wide enough to allow all possible values. It would seem useful to determine a measure of parameter sensitivity as a function of the range of allowed parameter values. However, as such a

measure depends strongly on the nature of the environment, and the values of the other parameters during the inversion, this measure has poor universality. Therefore, this avenue is not pursued in this thesis.

Increasing the number of iterations may also not be reasonable. In general, it is desirable to fix the amount of computational effort devoted to the problem and accept the best result after a given number of iterations. This is especially true in real-time problems, in which the best result in a given interval of time, and not the best result possible, is desired.

Freezing a parameter once the range of allowable values converges to within a pre-determined limit may also be problematic. What may be deemed a minute change in the value of one parameter may be more significant than a relatively large change in the value of another parameter. For example, in replicating the acoustic field, estimating the compressional velocity in the sediment to within ± 1 m/s is far more important than estimating the shear velocity in the bedrock to within an equal amount. Freezing a sensitive parameter with a small error may cause subsequent estimates of less sensitive parameters to contain a large error.

It is prudent not to bias the estimation of the lower sensitivity parameters by an arbitrary freezing criteria. The estimation of these parameters is a formidable task. The difficulty arises from the complexity of the search space for a matched field inversion problem. This complexity is illustrated by the extreme discontinuity in the correlation values of successively examined models. Numerous models, often with extremely different geoacoustic properties, produce similar acoustic fields sampled by a hydrophone array, and hence are associated with similar correlation values. As well, numerous models with only slightly different geoacoustic properties, produce markedly different acoustic fields, and hence are associated with different correlation values. The search space is replete with local optima.

The inter-relationship of the parameters in determining the acoustic field further complicates parameter estimation. These relationships may cause

parameters to converge in conjunction. For example, dense bottoms tend to support high shear wave velocities. In other cases, these relationships may cause parameters to converge to non-physical values as a compensation mechanism. For example, in the case of a head wave traveling at the bedrock interface, a deeper interface may cause the compressional velocity in the bedrock to be faster in order to compensate for the greater travel distance. In a richly multipath environment, such as the simulation environment, the cumulative effect is intractable.

The estimation of the values of the parameters with low sensitivities is especially difficult. The probability distributions of correlation values associated with relatively low sensitivity parameters show considerable variability during the inversion. Trends toward high correlation values associated with certain values of the less sensitive parameters tend to be overwhelmed by the effects of perturbations of the more sensitive parameters. There is generally an inadequate number of data points to average out these variations. However, as the sensitive parameters converge, the variability in correlation values decreases. The approximation of the N-dimensional parameter configuration space by N independent parameter spaces becomes increasingly justified, as the dimensions of the more sensitive parameters collapse to points. The probability distributions of correlation values of the lower sensitivity parameters begin to stabilize.

B. Uncertainty in the source/array geometry

The following two examples demonstrate the performance of the inversion algorithm when there is uncertainty in the assumed source/array geometry. This is a common situation in many field experiments. Errors in the source position of $^{+1}/_{3}$ and $^{-2}/_{3}$ of a wavelength are considered. As the wavelength of sound in sea water at 20 Hz is approximately 75 m, in the first example, it is assumed that the source is 25 m further than the actual range of 3000 m. In the second case, it is assumed that the source is 50 m closer.

The performance of the inversion algorithm is illustrated by figures 3.5 and 3.6. Figure 3.5, a plot of average correlation versus iteration contrasts the convergence properties of the inversion when there is an error in the assumed source/array geometry with the inversion performed with no error.

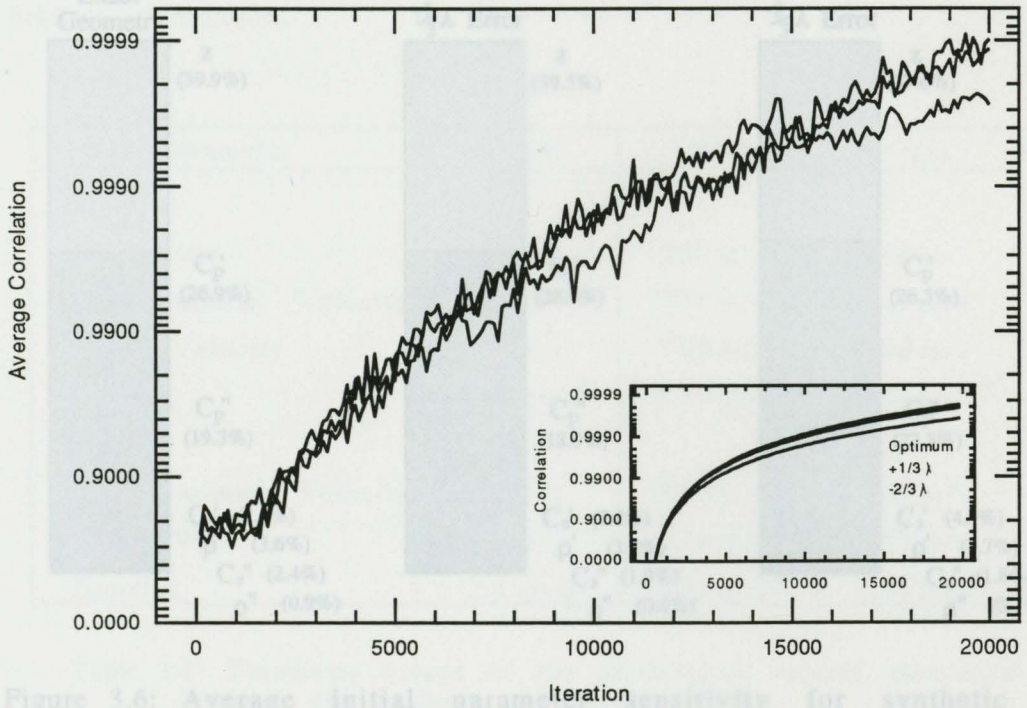

Figure 3.5: Average correlation versus iteration for synthetic inversions with an erroneous source location, compared with an inversion with exact source/array geometry.

In both inversions, the average correlation increased steadily, although not monotonically. With an error in the source location of $^{+1}/_{3}$ wavelength, the search converged to approximately 0.99989, only 0.00001 less than the value of 0.9999 for an inversion performed with an exact source/array geometry. With an error in the source location of $^{-2}/_{3}$ wavelength, the search converged to approximately 0.9998, only 0.0001 less than the value for an inversion performed with an exact source/array geometry. This indicates a near-exact replication of the acoustic field in each case.

Figure 3.6, a plot of the relative parameter sensitivity over the first 1500 iterations, contrasts the relative sensitivity for the inversions performed with an error in the source location, with the inversion performed with an exact source/array geometry.

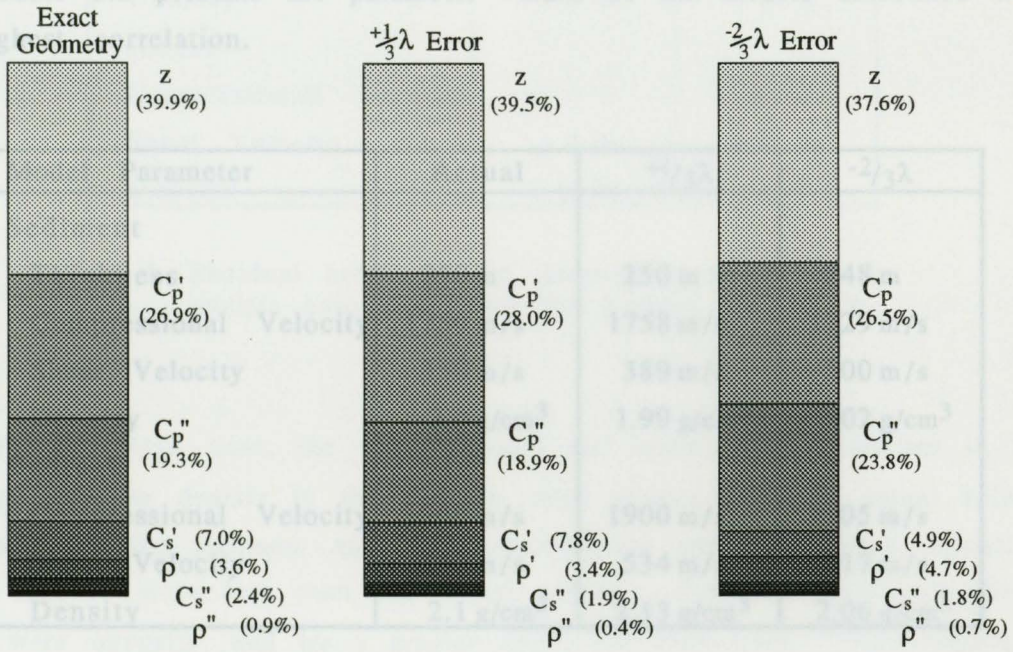

Figure 3.6: Average initial parameter sensitivity for synthetic inversions with an erroneous source location, compared with an inversion with exact source/array geometry.

The relative parameter sensitivities were very similar during the initial portion of all three inversions. This is to be expected given the similar nature of the inversions. It is probable that an inversion of a different environment would reveal significant differences in the relative sensitivities. However, some guidelines can be inferred: the acoustic field is very sensitive to layer depths; the field is increasingly insensitive to parameters characterizing successively deeper layers; and, the field is more sensitive to parameters determining the propagation of compressional waves than those determining the propagation of shear waves.

Initially, parameter sensitivities differed by two orders of magnitude. During the inversion, the parameter sensitivities decreased steadily, although not monotonically. By the end of the inversion, the parameter sensitivities differed by less than half an order of magnitude.

Table 3.2 presents the parameter values of the models associated with the highest correlation.

Model Parameter	Actual	$+1/3\lambda$	$-2/3\lambda$
Sediment			
Thickness	250 m	250 m	248 m
Compressional Velocity	1750 m/s	1758 m/s	1729 m/s
Shear Velocity	350 m/s	389 m/s	300 m/s
Density	2.0 g/cm^3	1.99 g/cm^3	2.02 g/cm^3
Bedrock			
Compressional Velocity	1900 m/s	1900 m/s	1905 m/s
Shear Velocity	550 m/s	534 m/s	617 m/s
Density	2.1 g/cm^3	2.13 g/cm^3	2.06 g/cm^3

Table 3.2: Parameter values of the geoacoustic models associated with the highest correlation.

The algorithm has been successful in determining the values of the unknown parameters, although less successful than in the case with absolute geometric certainty. The estimates of the thickness of the sediment layer and the compressional velocity in the bedrock remained quite accurate, the estimates of the compressional velocity in the sediment were moderately accurate, and the estimates of the other geoacoustic properties were least accurate.

Table 3.3 presents the residual errors in the parameter values for the models associated with the highest correlation.

Model Parameter	$+1/3\lambda$	$-2/3\lambda$
Sediment		
Thickness	0 %	- 1 %
Compressional Velocity	+ 8 %	- 11 %
Shear Velocity	+ 20 %	- 25 %
Density	- 5 %	+ 10 %
Bedrock		
Compressional Velocity	0 %	+ 3 %
Shear Velocity	- 8 %	+ 34 %
Density	+ 15 %	- 20 %

Table 3.3: Residual errors in the parameter values for the models associated with the highest correlation.

For the $+1/3\lambda$ case, the compressional and shear wave velocities in the sediment, and the density in the bedrock were greater than the actual values; the density in the sediment and the compressional and shear wave velocities in the bedrock were less than the actual values. For the $-2/3\lambda$ case, these results were opposite, and by a greater degree in each case. This implies a compensation mechanism.

i. Discussion

The correlation of the best model for the $+1/3\lambda$ case was 0.999965, and the correlation of the best model for the $-2/3\lambda$ case was 0.999964. In contrast, correlating the replica field associated with the actual environment, but with the erroneous source/array geometry leads to values of 0.993 and 0.943 respectively. The parameter values estimated by the inversion algorithm, therefore, more appropriately replicate the acoustic field measured at the horizontally shifted array, than the parameter values of the actual environment. Figure 3.7 illustrates the effect of an error in the source/array geometry.

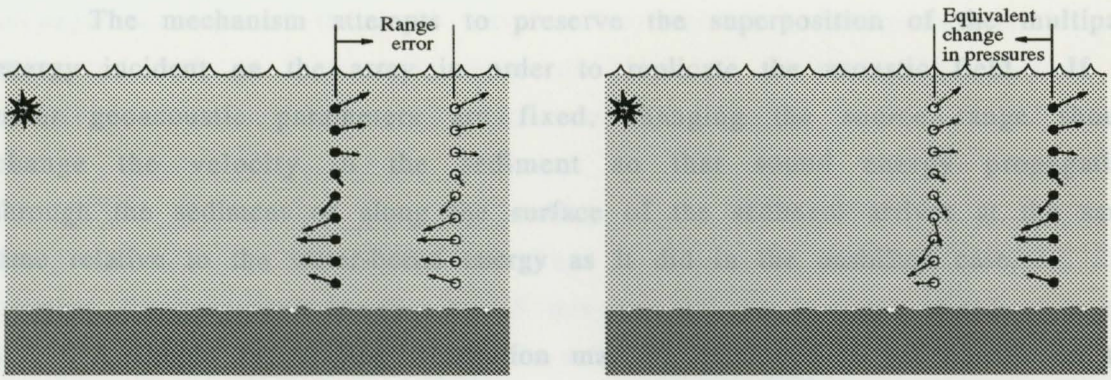

Figure 3.7: Introduction of an error in the source/array geometry.

The introduction of an error in the source/array geometry, as illustrated by the left portion of the figure 3.7, is equivalent to subtly altering the pressures at the actual hydrophone array location, illustrated by the right portion of figure 3.7.

An algorithm attempting to exactly reproduce these altered pressure vectors will not deduce the same geoacoustic environment. The inversion forces the parameters to converge toward values that better replicate the acoustic field at the hydrophone array, rather than simply making the task of converging toward values characteristic of the actual environment more difficult. A corollary to this conclusion is that if the geoacoustic parameters inferred to represent the ocean bottom are inaccurate, attempts at source localization will be degraded.

It is noteworthy that of the most sensitive parameters, the thickness of the sediment and the compressional velocities in the sediment and the bedrock, that only the estimate of the compressional velocity in the sediment is significantly in error. When the source is 25 m farther from the array, the compressional velocity is 8 m/s faster. When the source is 50 m closer to the array, the compressional velocity is 21 m/s slower. These results may be the result of a simple compensation relationship.

The mechanism attempts to preserve the superposition of the multipath energy incident on the array in order to replicate the acoustic field. If all other geoacoustic parameters are fixed, changing the source range should change the velocity in the sediment so that sound energy propagating through the sediment or along the surface of the sediment arrives at the same time relative to the water-borne energy as it did in the unshifted case.

A simple ray tracing illustration may be employed to set bounds on the error in estimating of the compressional velocity. Two rays, shown in figure 3.8, delineate the minimum and maximum change in the velocity.

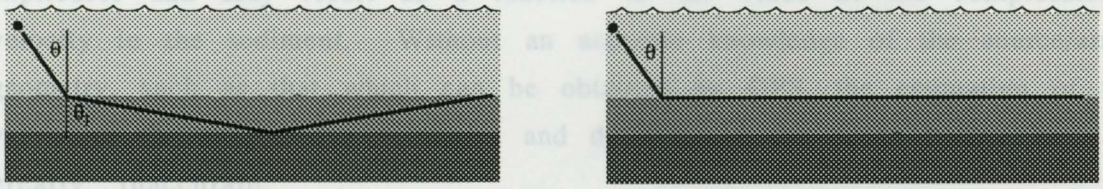

Figure 3.8: Ray paths delineating the minimum and maximum change in the compressional wave velocity in the sediment layer.

The necessary change in compressional velocity is related to the type of sound path and the path length. Depending on the path length, a modest change in the velocity of the medium can cause a drastic change in the arrival time. Limiting conditions for the velocity change can be derived from the following examples. The ray with one interface reflection within the sediment layer is illustrated on the left in figure 3.8. Given the experimental geometry, trigonometry may be used to determine the necessary change in compressional velocity for a given change in range. The increase in velocity associated with an increase in range of 25 m, is 0.5 m/s. The decrease in compressional velocity associated with a decrease in range of 50 m, is 1 m/s.

The ray with the shortest path within the sediment is the head wave along the sediment surface, as shown on the right in figure 3.8. The change in compressional velocity is directly proportional to the change in the

propagation range of the head wave. The increase in compressional velocity associated with an increase in range of 25 m, is 16 m/s. The decrease in compressional velocity associated with a decrease in range of 50 m, is 32 m/s.

For an increase in the source range of 25 m, the increase in compressional velocity, as estimated by the inversion, is 8 m/s, which lies between the estimated bounds of 0.5 m/s and 16 m/s. For a decrease in the source range of 50 m, the decrease in velocity, as estimated by the inversion, is 21 m/s, which lies between the estimated bounds of 1 m/s and 32 m/s.

The compensation mechanisms for the less sensitive parameters are less explicable and may result as a reaction to the value of the compressional velocity in the sediment. Without an accurate knowledge of the source/array geometry, such as that which can be obtained by GPS, the estimation of the values of the shear wave velocities and densities in the ocean bottom may be greatly inaccurate.

The inversion method obtains its power from its accurate modeling of the wave field. However, its accuracy makes it sensitive to uncertainty in the experimental geometry. The examples considered here have shown that although reasonably good parameter estimates were obtained, the performance was degraded for larger uncertainties.

C. Noise Contamination

The following two examples demonstrate the performance of the inversion algorithm when there is noise contamination, a situation arising in all field experiments. Noise was implemented by perturbing the pressures measured at the hydrophones by random amounts such that the power of the pressure divided by the power of the pressure plus the additive noise yielded a desired ratio averaged over the array. Signal-to-noise ratios of 20 dB and 10 dB are considered. Twenty decibels may be considered realistic for a short range,

shallow water experiment. Ten decibels may be considered a high degree of noise contamination.

The performance of the inversion algorithm is illustrated by figures 3.9 and 3.10. Figure 3.9, a plot of average correlation versus iteration contrasts the convergence properties of the inversion performed with noise contamination with the inversion performed in a noise-free environment.

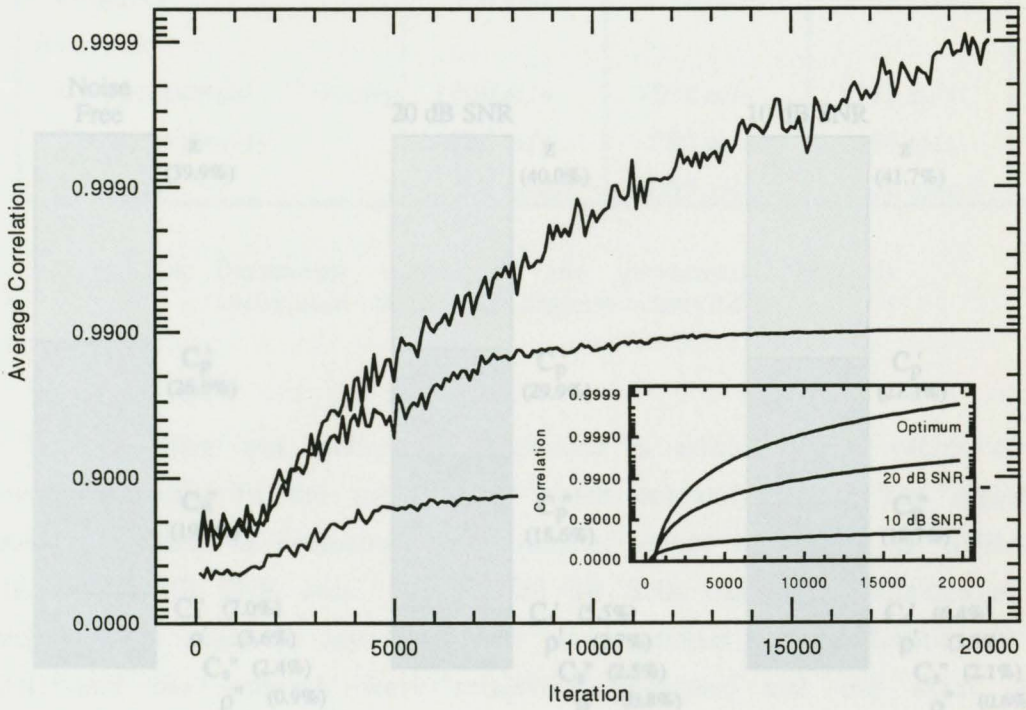

Figure 3.9: Average correlation versus iteration for synthetic inversions with noise contamination, compared with a noise-free inversion.

In both cases, the average correlation increased steadily, although not monotonically. With a SNR of 20 dB, the algorithm converged to approximately 0.99, about 0.01 less than the value of 0.9999 for an inversion performed in a noise-free environment. With a SNR of 10 dB, the algorithm converged to approximately 0.88, about 0.12 less than the value for an inversion performed

in a noise-free environment. This represents a significant degradation in the replication of the acoustic field.

Figure 3.10, a plot of the relative parameter sensitivity over the first 1500 iterations, contrasts the relative sensitivity for the inversions performed with noise contamination, with the inversion performed in a noise-free environment. The relative parameter sensitivities were very similar during the initial portion of all three inversions. This is to be expected given the similar nature of the inversions.

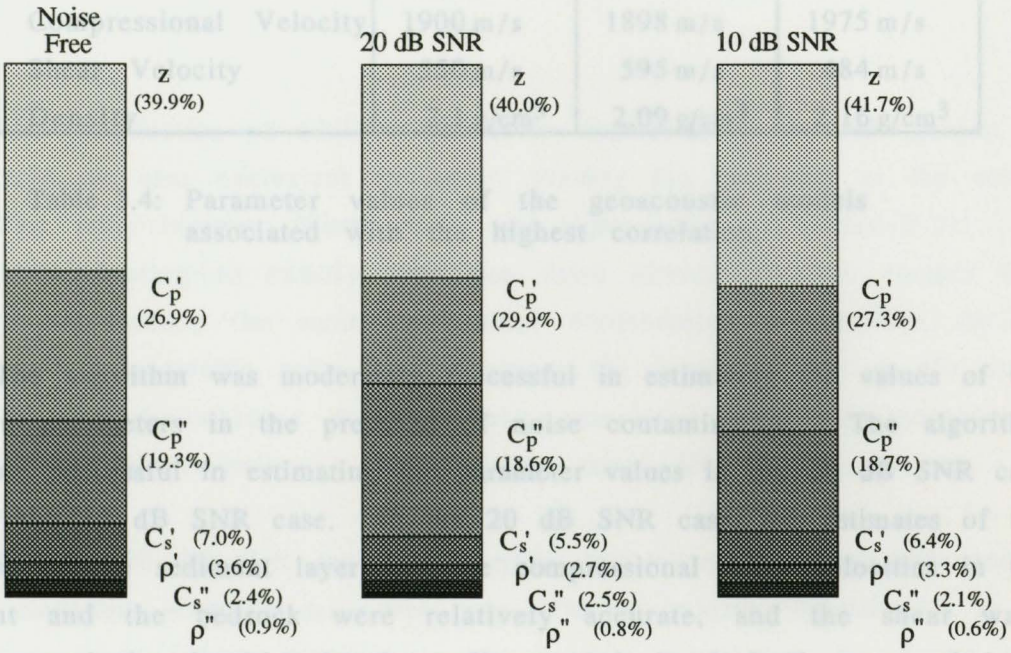

Figure 3.10: Average initial parameter sensitivity for synthetic inversions with noise contamination, compared with a noise-free inversion.

Initially, the parameter sensitivities differed by two orders of magnitude. During the inversion, the parameter sensitivities decreased steadily. By the end of the inversion, the parameter sensitivities differed by less than half an order of magnitude.

Table 3.4 presents the parameter values of the models associated with the highest correlation.

Model Parameter	Actual	20 dB SNR	10 dB SNR
Sediment			
Thickness	250 m	256 m	256 m
Compressional Velocity	1750 m/s	1750 m/s	1710 m/s
Shear Velocity	350 m/s	285 m/s	273 m/s
Density	2.0 g/cm^3	1.98 g/cm^3	2.09 g/cm^3
Bedrock			
Compressional Velocity	1900 m/s	1898 m/s	1975 m/s
Shear Velocity	550 m/s	595 m/s	484 m/s
Density	2.1 g/cm^3	2.09 g/cm^3	2.16 g/cm^3

Table 3.4: Parameter values of the geoacoustic models associated with the highest correlation.

The algorithm was moderately successful in estimating the values of the unknown parameters in the presence of noise contamination. The algorithm was more successful in estimating the parameter values in the 20 dB SNR case than in the 10 dB SNR case. In the 20 dB SNR case, the estimates of the thickness of the sediment layer and the compressional wave velocities in the sediment and the bedrock were relatively accurate, and the shear wave velocities and the densities in the sediment and the bedrock were relatively inaccurate. In the 10 dB SNR case, the estimation of the thickness of the sediment layer was relatively accurate, but the estimations of the other parameters were largely inaccurate.

i. Discussion

The effect of the noise contamination on parameter estimation is quite drastic. Figure 3.11 illustrates the effect of introducing additive noise.

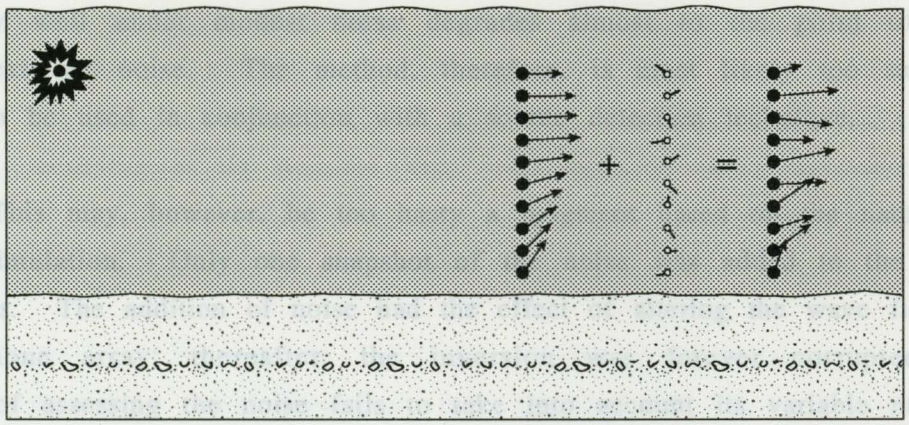

Figure 3.11: Introduction of additive noise.

The introduction of additive noise, as illustrated by the left portion of figure 3.11, is also equivalent to subtly altering the pressures at the actual hydrophone array location, illustrated by the right portion of figure 3.11. An algorithm attempting to exactly reproduce these altered pressure vectors will therefore not deduce the same geoacoustic environment. Therefore, in the presence of considerable noise contamination, the acoustic field at the array will bear no resemblance to the field associated with the geoacoustic properties of the environment. The inversion may yield invalid results.

For the 20 dB SNR case, the average correlation drops an order and a half of magnitude from the noise-free case. Further reducing of the SNR to 10 dB results in a further decrease in the average correlation by almost two orders of magnitude.

The 20 dB SNR example illustrates the sensitivity of the inversion method to realistic noise conditions. The algorithm performed relatively well under the addition of a realistic level of background noise. The method may, therefore, be well suited as an operational survey technique.

The 10 dB SNR example illustrates the sensitivity of the inversion method to an extremely noisy environment. The algorithm that performed

passably well under modest noise degrades almost to the point of inutility under extreme noise. The method, therefore, is most likely too sensitive to noise to be used in conjunction with a source detection technique.

This may, however, be too hasty a judgment based on the nature of the noise simulation. Only one snapshot of the noise was added to the measured pressures. The addition of noise had the effect of altering the wave field at the hydrophone array; thereafter, the inversion was forever corrupted. This means of assessing the noise fails to take into account its variable nature. In an actual scenario, several pressure measurements may be made, and the noise contamination reduced using signal processing techniques.

IV. Summary

The successful inversions of the synthetic environment demonstrated the feasibility of the method developed in the previous chapter. The first inversion, performed under optimum conditions: a noise-free environment and absolute geometric certainty, demonstrated that the method was very successful in estimating the values of the unknown parameters. The second two inversions, performed with an error in the source position, demonstrated the dependence of the method on an accurate knowledge of the source/array geometry. The final two inversions, performed under noise contamination, demonstrated the dependence of the method on the accurate measurement of the acoustic field at the hydrophone array.

The inversion method obtains its power from its accurate modeling of the wave field. In a richly multipath environment, such as shallow water, the combinations of geoacoustic parameters that can create a semblance of the desired acoustic field sampled by a hydrophone array are practically infinite. The inversion for the globally optimum parameter configuration is a formidable task.

Under idealized conditions, a noise-free environment with absolute geometric certainty, the accuracy of the wave field modeling allows it to robustly converge toward the exact solution. However, the accuracy of the acoustic modeling is its Achilles heel. In such an under-determined system, altering the solution even slightly causes an inversion to determine a vastly different set of geoacoustic parameters.

Both the uncertainty in the source/array geometry and noise contamination are equivalent to the altering of the pressures at the hydrophone array. When these effects are significant, therefore, the inversion will converge to an erroneous set of geoacoustic parameters.

It is important to note that although the simulations have shown the inherent weakness of the inversion method, reasonably good parameter estimates were obtained for a moderate uncertainty in the source position and a realistic level of background noise.

Chapter 4

Experimental Study

I. Data Collection

Acoustic field data was collected in an experiment conducted by the Defence Research Establishment Pacific, from April 24 to 25, 1985. The experimental configuration is shown in figure 4.1. The experiment was conducted in relatively shallow water, approximately 200 m depth, overlying a relatively flat bottom. Acoustic sources were detonated at approximately 20 m depth, in range increments of two kilometers. The resulting acoustic field was sampled by a multi-element vertical line array spanning the lower half of the water column. The research vessel CFAV Endeavour monitored the array while the CSS Parizeau jettisoned the explosive charges. The pressures measured at the array from the closest shot were used to estimate the local geoacoustic properties.

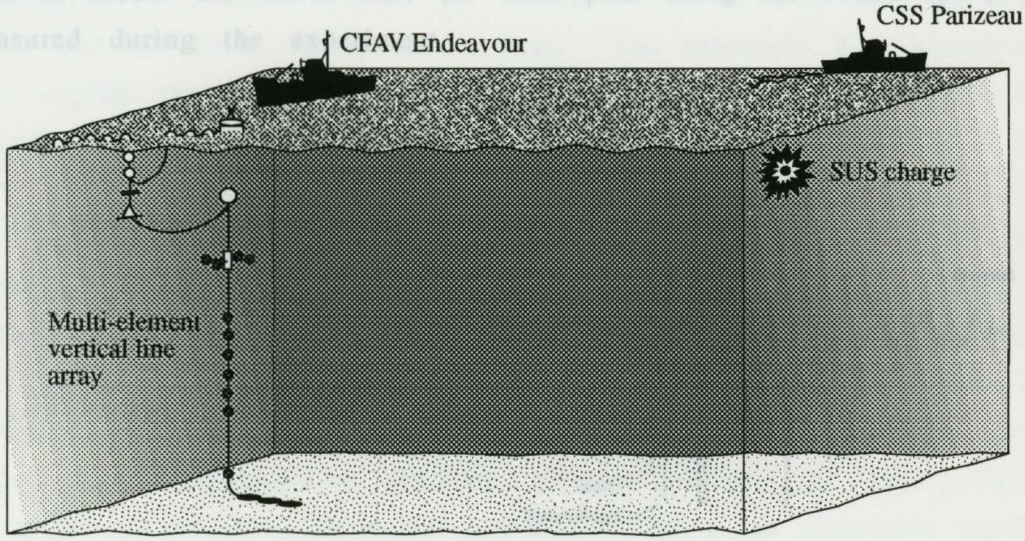

Figure 4.1: Experimental configuration for an experiment conducted by the Defence Research Establishment Pacific in April 1985.

The hydrophone array was composed of seven main parts:

- a surface float, containing a radar transponder and reflector, the surface electronics unit, and the FM radio link;
- a damper plate to isolate the array from surface waves;
- a sub-surface float from which the array was suspended;
- the lower electronics unit, containing the power gain amplifier, digitizer, tilt sensor, and multiplexor;
- a horizontal circular array;
- a multi-element vertical array; and,
- weights to hold the array in a vertical attitude.

Ten hydrophones were used to sample the pressure field at 82 m depth, in 6 m intervals from 101 m to 143 m, and at 196 m depth. The source depth was 24 m, as determined by standard techniques (Chapman, 1988). The source range was 1.48 ± .02 km, as estimated using ray theory, as shown in figure 4.2. The difference in travel time between the direct ray path and the first bottom bounce was used as a measure of the range. The travel time difference was modeled at incremental ranges in order to estimate the range corresponding to the measured time difference. The Generic Sonar Model (Weinberg, 1985) was used to model the travel time for each path using the sound speed profile measured during the experiment.

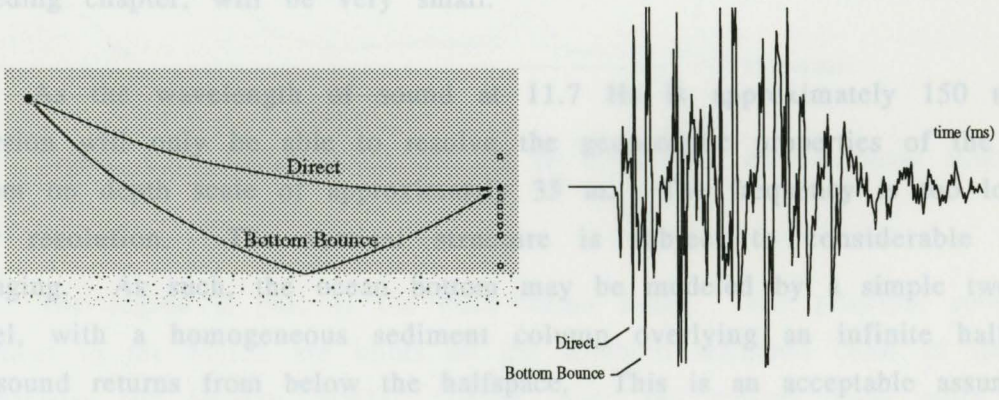

Figure 4.2: Estimation of the source range using ray-tracing.

As the source/array geometry is known to within approximately $\pm 1/4$ wavelength of sound (at 12 Hz), the effect of a range error on parameter estimation, as demonstrated in the preceding chapter, will be relatively small.

II. Data Processing

Data from the hydrophones in the band 0-500 Hz were sampled at 1500 Hz, sub-multiplexed along with the array status information, and transmitted to CFAV Endeavour by an FM radio link. The data were recorded on magnetic tape.

To form the covariance matrix of the pressures measured at the array, a fast Fourier transform of the shot's wave form was performed at each hydrophone, and the cross spectral matrix was formed at 11.7 Hz. The low frequency was chosen to take advantage of the maximum spectral power for shallow shots. For 20 m depth shots, the spectral peak is about 10 Hz.

The signal-to-noise ratio along the hydrophone array at 11.7 Hz was approximately 50 dB. Figure 4.2 illustrates the contrast between the shot power and the noise of the environment. The extremely high signal-to-noise ratio implies that the effects of noise contamination, as demonstrated in the preceding chapter, will be very small.

As the wavelength of sound at 11.7 Hz is approximately 150 m, the inversion will only be able to resolve the geoacoustic properties of the ocean bottom on depth scale of approximately 35 m. The frequency is too low for finer resolution. The vertical structure is subject to considerable spatial averaging. As such, the ocean bottom may be modeled by a simple two-layer model, with a homogeneous sediment column overlying an infinite halfspace. No sound returns from below the halfspace. This is an acceptable assumption, as any such reflected energy would be strongly attenuated, and the range is too small (relative to the frequency) to permit the return of refracted energy.

III. Geoacoustic Environment

A. Regional Geological Framework

The experiment was conducted at a site on the edge of the continental shelf off the west coast of Vancouver Island, Canada, as shown in figure 4.3.

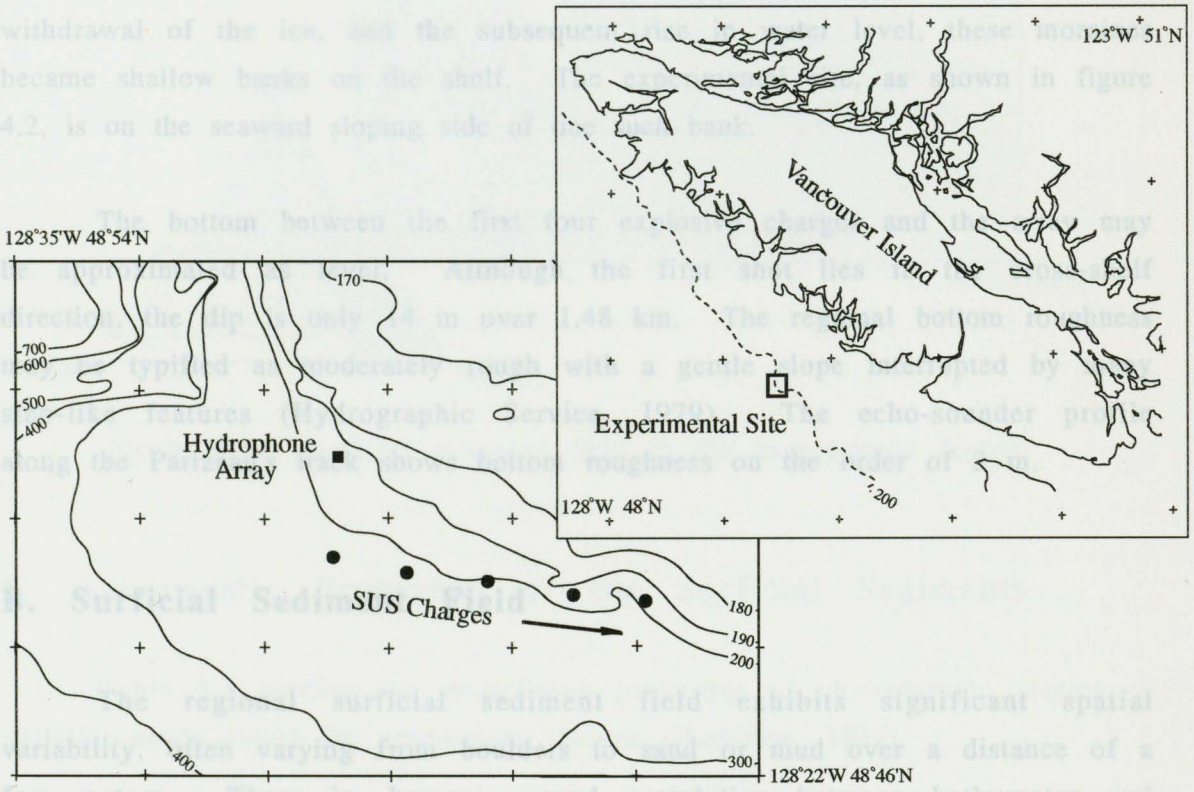

Figure 4.3: Experimental site off the west coast of Vancouver Island.

The region is part of the Fuca-Tofino Basin. The principal sources of sediment to the region are inlets on the southern mainland coast of the shelf (Luternauer and Murray, 1983). Relict sands and gravels cover most of the shelf. This cover was initially dispersed by glaciers and meltwater streams, then later inundated during the Holocene Transgression, and now is being

partly reworked by the present hydraulic regime (Carter, 1973). Sediments in this basin have had variable uplift/subsidence and reworking histories. The near-surface sediment is predominantly composed of immature marine siltstone, shale, and minor sandstone (Shouldice, 1973). The spatial variability in bedforms is considerable, due to reworking (Bornhold and Yorath, 1983).

During recent periods of glaciation, ice sheets covered much of the shelf. The movement of glaciers gave rise to gravelly moraines. With the withdrawal of the ice, and the subsequent rise in water level, these moraines became shallow banks on the shelf. The experimental site, as shown in figure 4.2, is on the seaward sloping side of one such bank.

The bottom between the first four explosive charges and the array may be approximated as level. Although the first shot lies in the cross-shelf direction, the dip is only 14 m over 1.48 km. The regional bottom roughness may be typified as moderately rough with a gentle slope interrupted by many step-like features (Hydrographic Service, 1979). The echo-sounder profile along the Parizeau's track shows bottom roughness on the order of 3 m.

B. Surficial Sediment Field

The regional surficial sediment field exhibits significant spatial variability, often varying from boulders to sand or mud over a distance of a few meters. There is, however, good correlation between bathymetry and sediment texture (Herzer and Bornhold, 1982). On the tops of shallow banks, well stratified, consolidated gravels are found in high concentrations. Where the sloping bank is exposed to the open ocean, the gravel facies give way to clean sand, which in turn becomes muddier toward the shelf edge. Figure 4.4 illustrates the surficial sediment field in the experimental region, which lies across the seaward side of a shallow sloping bank.

The surficial sediments between the first shot and the hydrophone array may be inferred to have a 50-90% sand content ($\rightarrow$ 90%), 10-50% mud

content (→10%), and 30-80% gravel content, (→30%). These sediments may be classified as gravelly muddy sand.

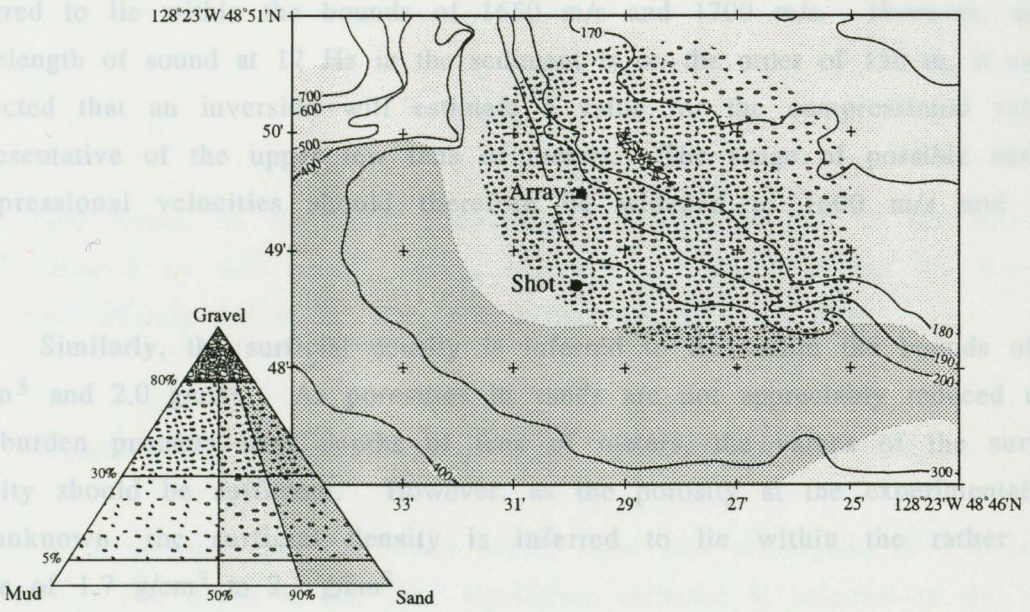

Figure 4.4: Surficial sediment field in the experimental region.

C. Geoacoustic Properties of the Surficial Sediments

Table 4.1 typifies the geoacoustic properties of characteristic classes of surficial sands found on continental shelves (Hamilton, 1987).

Sand	% Sand	Compress. Velocity	Density
Coarse	100.0	1806 m/s	2.034 g/cm^3
Fine	92.2	1705 m/s	1.962 g/cm^3
Very fine	81.0	1658 m/s	1.878 g/cm^3
Silty	57.0	1608 m/s	1.783 g/cm^3

Table 4.1: Geoacoustic properties for characteristic classes of sands in continental terrace sediments. From Hamilton, 1987.

The compressional velocities in the table have been corrected for a local bottom water velocity of 1480 m/s. As the surficial sediments are inferred to have a sand content of 50-90% ($\rightarrow$90%), the surficial compressional velocity is inferred to lie within the bounds of 1650 m/s and 1700 m/s. However, as the wavelength of sound at 12 Hz in the sediment is on the order of 150 m, it can be expected that an inversion will estimate a value for the compressional velocity representative of the upper few tens of meters. The range of possible surficial compressional velocities should therefore be widened to 1600 m/s and 1800 m/s.

Similarly, the surficial density is inferred to lie within the bounds of 1.8 g/cm^3 and 2.0 g/cm^3. As porosities in sands are not appreciably reduced under overburden pressure over depths of tens of meters, the values of the surficial density should be sufficient. However, as the porosity at the experimental site is unknown, the surficial density is inferred to lie within the rather wide range of 1.7 g/cm^3 to 2.1 g/cm^3.

Representative estimates of the value of the shear velocity in the surficial sediment are less reliable as there have been few *in situ* measurements in marine sediments (Hamilton, 1987). Although shear velocities generally approach zero at the sea floor, they increase rapidly over the first few tens of meters depth (Ohta and Goto, 1978; Hamilton, 1976). Therefore, realistic bounds on the surficial shear velocity should be representative of the upper few tens of meters. Compressional velocity and shear velocity have been linked through a regression equation by Hamilton (1979). According to this equation, for compressional velocities between 1600 m/s and 1800 m/s, the shear velocities should vary between 375 m/s and 475 m/s. However, surficial shear velocities of up to 580 m/s in fine sands have been quoted in the literature (Hamilton, 1976). The surficial shear velocity is therefore inferred to lie within the bounds of 350 m/s and 550 m/s.

Due to the lack of low frequency measurements, realistic bounds on the compressional attenuation are difficult to set. As such, compressional attenuation is inferred to lie within the rather liberal bounds, 0.25 dB/λ to 0.75

dB/λ (Stoll, 1986; Hamilton, 1987). Although high values of the shear attenuation are quoted in the literature, the theoretical acoustic propagation model used (SAFARI) constrains the shear attenuation to be less than or equal to the bound,

$$\alpha_s \leq \frac{3}{4}\left(\frac{C_p}{C_s}\right)^2 \alpha_p \, .$$

The upper bound on the shear attenuation was therefore set to the maximum value allowed by this bound, which, although it changed during the inversion was approximately 5.0 dB/λ. The lower bound was set to 1.0 dB/λ.

D. Geoacoustic Properties of the Sediments at Depth

It is assumed that the lower model layer will correspond to a reflection boundary. The depth to the first significant reflector is inferred to lie within the bounds of 50 m and 200 m. Although there are probably several reflectors within this range, the inversion will attempt to find the depth to the most significant reflector within this range.

Bounds on the compressional velocity at the reflector may be inferred from sonic log data from an exploratory well drilled in the vicinity, figure 4.5.

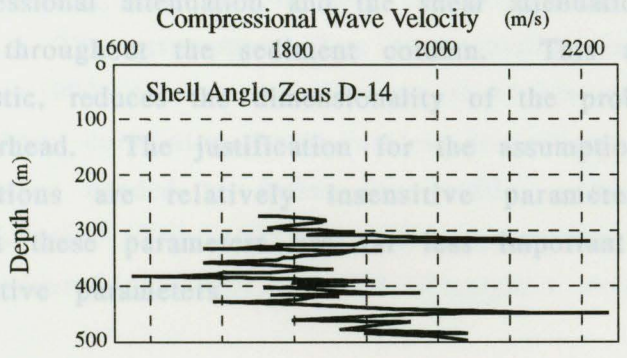

Figure 4.5: Sonic log velocity versus depth profile for Shell Anglo exploratory well Zeus D-14.

The compressional velocity in the reflector is inferred to lie within the bounds of 1900 m/s and 2100 m/s. However, as the compressional velocity is quite variable on a depth scale much smaller than the wavelength of sound being considered, it may be anticipated that the estimation of the compressional velocity at the reflector may be smeared over a large range.

The lowest value of the shear velocity in the sediment is significant in determining the amount of sound energy trapped in the water column. The lower the shear velocity, the less energy is trapped, and the poorer is long range propagation. Therefore, the bounds on the shear velocity at the reflector are set to bracket the most probable lowest value of the shear velocity, 200 m/s to 400 m/s. It is important to note that when the data were inverted and the shear velocity at depth was allowed to assume any value between 200 m/s and 1000 m/s, there was a steady decrease in correlation associated with higher values of the shear velocity. These results support the assumption of low shear velocities.

The density at the reflector may be inferred from empirical relationships between density and compressional velocity, which contain a 'built in' pressure correction. On the basis of a regression equation linking density to compressional velocity in semi-lithified mudstone (Hamilton, 1977), the density at the reflector is inferred to lie within the bounds of 1.9 g/cm^3 and 2.3 g/cm^3.

The compressional attenuation and the shear attenuation are assumed to be homogeneous throughout the sediment column. This assumption, though physically unrealistic, reduces the dimensionality of the problem and thus the computational overhead. The justification for the assumption lies in the fact that the attenuations are relatively insensitive parameters. Constraining assumptions about these parameters are far less important than assumptions about more sensitive parameters.

E. Acoustic Properties of the Water Column

Figure 4.6 illustrates sound velocity profiles in the water column taken during the experiment. The left profile was obtained by CSS Parizeau 20 km in the along-shelf direction during the shot run and the middle profile obtained 20 km oceanward the previous day. The right profile, inferred from the other two, was taken as representative of the experimental region.

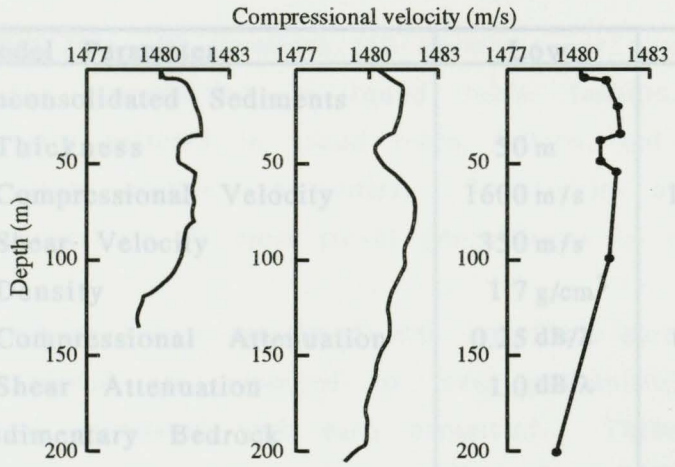

Figure 4.6: Variation of compressional velocity with depth in the experimental region.

The velocity profile taken as representative of the experimental region was based on the along-shelf profile, and extrapolated to 200 m using the cross-shelf profile. The assumption of a representative profile is reasonable in light of Zeller's (1990) conservative estimates of 45 km and 27 km as along-shore and cross-shore correlation length scales, respectively. Nine layers is the minimum number needed to define the profile. Density is considered constant at 1.022 g/cm^3 (Gill, 1982), a valid assumption in shallow water. Attenuation is considered negligible, a valid assumption over short ranges.

IV. The Inversion Algorithm

The inversion algorithm attempts to estimate the geoacoustic properties of the ocean bottom. The parameter search space of geoacoustic models is defined as the continuum in nine dimensions bound by the permissible ranges of the unknown parameters as inferred from geological reasoning. Table 4.2 presents the permissible ranges of the unknown parameters.

Model Parameter	Low	High
Unconsolidated Sediments		
Thickness	50 m	200 m
Compressional Velocity	1600 m/s	1800 m/s
Shear Velocity	350 m/s	550 m/s
Density	1.7 g/cm^3	2.1 g/cm^3
Compressional Attenuation	0.25 dB/λ	0.75 dB/λ
Shear Attenuation	1.0 dB/λ	~5.0 dB/λ
Sedimentary Bedrock		
Compressional Velocity	1900 m/s	2100 m/s
Shear Velocity	200 m/s	400 m/s
Density	1.9 g/cm^3	2.3 g/cm^3

Table 4.2: Ranges of geoacoustic model parameters.

The inversion is initialized by assigning the parameters random values from within these ranges. The parameter configuration is iteratively perturbed by reassigning individual parameter values from these ranges.

For each perturbed model, the acoustic field that would be measured at the hydrophone array is computed using the fast field solution calculated by the SAFARI program (Schmidt, 1990). These replica acoustic fields are correlated with the measured acoustic field, stored as the covariance matrix of

the pressures measured at the hydrophone array. The correlation is computed by the Bartlett beamformer.

Parameter reconfigurations that increase the correlation are accepted unconditionally. Perturbations that decrease the correlation are accepted with probabilities assigned by a Boltzmann probability distribution, scaled by assigning a 50% probability of accepting a decrease in correlation of zero, and a 40% probability of accepting an average magnitude decrease in correlation.

During the first 450 iterations (50 iterations per parameter), parameters are selected for perturbation in round robin fashion. Subsequently, parameters are still selected in round robin fashion, but with probabilities proportional to their relative sensitivities. Sensitivities are calculated from moving-averages over the 50 most recent perturbations of each parameter.

The correlation values associated with individual parameter values from each model explored are averaged to form probability distributions of correlation values associated with each parameter. These distributions are computed by fitting the data in each dimension with a seventh-order polynomial. Seven orders was deemed adequate to represent a strongly multimodal parameter space of low dimensionality, while maintaining a high degree of data smoothing.

The search is gradually restricted to preferentially examine models associated with high values of the correlation using the weighting method described in chapter two. Initially, parameters are chosen with equal probability. Subsequently, the parameters are chosen based on an evolving probability distribution. The weighting function doubles the probability of perturbing a parameter to a value associated with an above-average value of correlation every 1800 iterations (200 iterations per parameter). Therefore, more sensitive parameters, and those parameters that display more significant clustering of high correlation values converge more rapidly.

the pressures measured at the hydrophone array. The correlation is computed by the Bartlett beamformer.

Parameter reconfigurations that increase the correlation are accepted unconditionally. Perturbations that decrease the correlation are accepted with probabilities assigned by a Boltzmann probability distribution, scaled by assigning a 50% probability of accepting a decrease in correlation of zero, and a 40% probability of accepting an average magnitude decrease in correlation.

During the first 450 iterations (50 iterations per parameter), parameters are selected for perturbation in round robin fashion. Subsequently, parameters are still selected in round robin fashion, but with probabilities proportional to their relative sensitivities. Sensitivities are calculated from moving-averages over the 50 most recent perturbations of each parameter.

The correlation values associated with individual parameter values from each model explored are averaged to form probability distributions of correlation values associated with each parameter. These distributions are computed by fitting the data in each dimension with a seventh-order polynomial. Seven orders was deemed adequate to represent a strongly multimodal parameter space of low dimensionality, while maintaining a high degree of data smoothing.

The search is gradually restricted to preferentially examine models associated with high values of the correlation using the weighting method described in chapter two. Initially, parameters are chosen with equal probability. Subsequently, the parameters are chosen based on an evolving probability distribution. The weighting function doubles the probability of perturbing a parameter to a value associated with an above-average value of correlation every 1800 iterations (200 iterations per parameter). Therefore, more sensitive parameters, and those parameters that display more significant clustering of high correlation values converge more rapidly.

The probability distributions become increasingly stable as the parameters converge. As the values of each parameter are selected increasingly frequently from values associated with above-average values of correlation, the sensitivity of all the parameters approaches a small number. As such, averaging of correlation values of a particular parameter allows the parameter's probability distribution to be approximated as if all the other variables were essentially constant. This allows the preferential selection of parameter values associated with above average values of correlation for even low sensitivity parameters. By only storing the probability distributions and not the models themselves, the computational overhead is thus reduced.

V. Results

The performance of the inversion algorithm on field data is presented in figure 4.7, a plot of the probability distributions of the correlation associated with the values of each parameter at iteration 20000.

The maximum correlation associated with the peak of each probability distribution converged to 0.975 by iteration 20000. As the probability distributions were averaged over 20000 values, the peaks of the distributions correspond to the optimum parameter values. The error in the estimation may be taken as the width of the distribution above the average change in correlation per perturbation at iteration 20000. This range must include the optimum parameter value.

Averaging over 20000 iterations allowed the probability distributions of even the low sensitivity parameters to stabilize. A general unimodal structure is apparent in all the parameters except the sediment thickness, which is strongly bimodal. This may result from the fact that the sediment thickness determines the interference of reflected energy from the ocean/sediment interface and the sediment/bedrock interface.

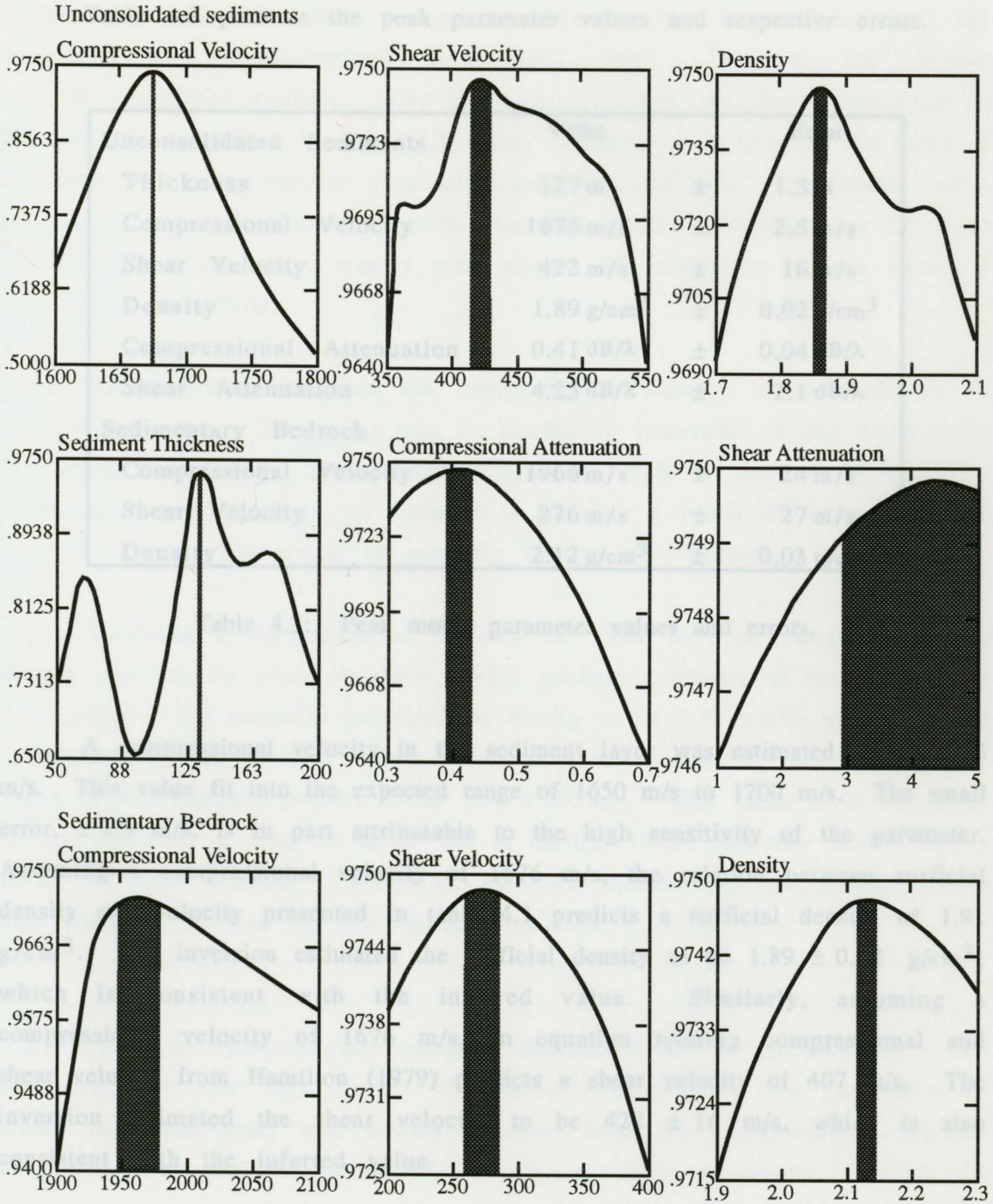

Figure 4.7: Probability distributions of geoacoustic model parameters at the 20000th iteration.

Table 4.3 presents the peak parameter values and respective errors.

	Value		Error
Unconsolidated Sediments			
Thickness	127 m	±	1.5 m
Compressional Velocity	1676 m/s	±	2.5 m/s
Shear Velocity	422 m/s	±	16 m/s
Density	1.89 g/cm^3	±	0.02 g/cm^3
Compressional Attenuation	0.41 dB/λ	±	0.04 dB/λ
Shear Attenuation	4.25 dB/λ	±	2.1 dB/λ
Sedimentary Bedrock			
Compressional Velocity	1966 m/s	±	24 m/s
Shear Velocity	276 m/s	±	27 m/s
Density	2.12 g/cm^3	±	0.03 g/cm^3

Table 4.3: Peak model parameter values and errors.

A compressional velocity in the sediment layer was estimated to be 1676 m/s. This value fit into the expected range of 1650 m/s to 1700 m/s. The small error, ± 2.5 m/s, is in part attributable to the high sensitivity of the parameter. Assuming a compressional velocity of 1676 m/s, the relation between surficial density and velocity presented in table 4.1 predicts a surficial density of 1.91 g/cm^3. The inversion estimated the surficial density to be 1.89 ± 0.02 g/cm^3, which is consistent with the inferred value. Similarly, assuming a compressional velocity of 1676 m/s, an equation relating compressional and shear velocity from Hamilton (1979) predicts a shear velocity of 407 m/s. The inversion estimated the shear velocity to be 422 ± 16 m/s, which is also consistent with the inferred value.

Assuming a surficial density of 1.89 g/cm^3, an equation relating attenuation and density (Hamilton, 1972; through porosity Akal, 1972) predicts a compressional attenuation of 0.8 dB/λ. The inversion estimated the compressional attenuation to be 0.41 ± 0.04 dB/λ. However, recent studies of

attenuation in the frequency range from 10 to 250 Hz indicate that the attenuation may be significantly lower (Stoll, 1986). Therefore, the estimate may be considered realistic. The inversion estimated the shear attenuation in the sediment column to be 4.1 ± 2.1 dB/λ. A shear attenuation on the order of ten times the compressional attenuation may be considered a reasonable value for compacted sands (Meissner, 1965; Hamilton, 1980). However, as the least sensitive parameter, there was a great degree of uncertainty in the value of the shear attenuation.

The inversion estimated the compressional velocity in the reflector to be 1966 ± 24 m/s. This value may be considered reasonable if one extrapolates the velocities from the Shell Anglo exploratory well to shallow depth. The considerable uncertainty in the velocity is possibly a result of the inability of the low-frequency inversion to spatially resolve the reflector.

Assuming a compressional velocity of 1966 m/s, an equation relating density and velocity from Hamilton (1977) predicts a density at the reflector of 2.08 g/cm^3. The inversion estimated the density to be 2.12 ± 0.03 g/cm^3, which is consistent with inferred value. The inversion estimated the lowest shear speed in the sediment column to be 276 ± 27 m/s. This value is a reasonable average value at a depth of about 100 m (Smith, 1986), and may result from a layer with low velocity. There is, however, considerable uncertainty, which may have arisen from the low spatial resolution.

Table 4.4 presents the average sensitivities of the parameters. The parameters fit into four classes of relative sensitivity. The parameters to which the beamformer was acutely sensitive were the compressional velocity in the sediment and the depth to the reflector. The parameters to which the beamformer was modestly sensitive were the compressional velocity in the underlying reflector, the surficial shear velocity and the attenuation in the sediment. The parameters to which the beamformer was relatively insensitive were the densities and the lowest shear velocity in the sediment column.

Variations in the shear attenuation caused essentially negligible changes in the beamformer output.

Unconsolidated Sediments	Relative Sensitivity
Thickness	37.4
Compressional Velocity	54.6
Shear Velocity	1.3
Density	0.7
Compressional Attenuation	1.3
Shear Attenuation	0.1
Sedimentary Bedrock	
Compressional Velocity	4.0
Shear Velocity	0.3
Density	0.4

Table 4.4: Average parameter sensitivity.

V. Discussion

The method was successful in estimating the geoacoustic properties of the ocean bottom and underlying sediment and bedrock at the experimental site. The geoacoustic parameters comprising the representative model were reasonable, consistent with inferred values from other techniques, and mutually consistent with the values of the other model parameters.

The estimation of the acoustic field was most sensitive to the compressional velocity at the ocean/sediment interface. This is consistent with the effect this interface has on the propagation of the waterborne acoustic energy. The surficial shear speed is similarly important, as it effects a significant loss mechanism. At interfaces, incident compressional energy may be converted to shear waves, which are subject to a much greater attenuation. The density at the ocean/sediment interface is not as important.

This is partly because the range of possible density values, ± 0.2 g/cm^3, was much less than the density contrast, approximately 1.0 g/cm^3.

The most critical sub-bottom parameter is the depth to the reflector. The thickness of the sediment above the reflector determines the path length of reflected sound, and thereby plays a significant role in determining the degree of attenuation of the sound returned from the sub-bottom. Performing the inversion at greater ranges would allow source localization to be less dependent on the geoacoustic properties of the sub-bottom, as much of the energy returning by such paths would be more strongly attenuated.

One must be suspicious of accepting estimates of the parameter values of the reflector out-of-hand. Direct ray and bottom-bounce paths determine the acoustic field at the hydrophone array to the first order. The search algorithm assigns sub-bottom parameter values as a second order correction to the wave field. It is possible that the search algorithm may compensate for any errors in the first order approximation of the wave field, due to an erroneous assumption of the source/array geometry or noise at the array, by assigning unrealistic values to the parameters characterizing the lower reflection boundary.

In the inversion on the data presented, this does not appear to be the case. Evidence for this is the high correlation of the replica acoustic field (0.975) and the reasonable and consistent parameter values at the reflector. Although this inversion was a success, caution must be exercised in applying any over-simplified model representation to reality. The search algorithm is only loosely constrained to accept reasonable parameter configurations. Its primary purpose is to match the pressures at the hydrophones by assigning parameter values in any manner permitted. The fact that the inversion was successful in such an extremely non-linear environment attests to the power of the self-guided, randomized search method, coupled to the precision of the matched field method and the acoustic propagation model.

Chapter 5

Conclusions and Suggestions for Future Research

A. Conclusions

A method was developed for the estimation of geoacoustic model parameters by the inversion of acoustic field data. The method is both accurate and robust. Accuracy is achieved by modeling the full wave field, and robustness is achieved by using an efficient, self-guided search algorithm.

The principal advantage of this method over conventional parameter estimation techniques is its capability of estimating near-surface geoacoustic properties, as well as those of deeper layers. The near surface properties are generally not recovered in standard seismic inversion. As well, the inversion method is capable of estimating shear wave properties. Shear wave properties are also not generally estimated by most seismic methods.

Implementation of the inversion method is relatively straightforward. A geoacoustic model representation of the ocean bottom is inferred, and a suite of models are used to compute replica fields, which are correlated with a measured field using a Bartlett matched field processor. A search algorithm is used to search the parameter space for the model associated with the highest correlation. Frustration by locally optimal models is avoided by the use of probabilistic transition operators. The need for pre-determination of the control parameter that scales the topographic variability of the parameter space is eliminated using a feedback loop. The search is made more efficient by weighting parameter selection by relative parameter sensitivity. The search is made self-guiding using historic information to concentrate on regions of the parameter space that are associated with above-average correlation values.

The method is relatively simple to generalize to any combinatorial optimization problem. The control parameters are chosen by statistical consideration, rather than the nature of the problem. The inversion method, can therefore accommodate different or more complex problems. Although the assumptions on which it operates are increasingly valid in low-dimension problems or high-dimension problems with considerable variation in parameter sensitivity, the algorithm only guides the search in proportion to the strength of the trends in correlation apparent in the data. For an inversion problem exhibiting only weak trends in correlation, the search will lose some extra efficiency afforded by the guidance, but it will not fail.

The method is appropriately cast for real-time operation. The method yields the best solution possible in a given amount of time. In each time interval, the inversion should yield the best estimate of the geoacoustic parameters naturally inferred from the models examined. As well, the method is not constrained to selecting one of the examined parameter configurations. The method averages the best parameter values from each model examined.

The method is also appropriately cast for *in situ* operation. It is adaptable to any ocean environment, with minor alteration of the ranges of the geoacoustic parameters. If the values of the geoacoustic properties of the environment change with time, as would be noted from a moving sensor platform, the method is able to adapt, without operator guidance. A significant drawback is the time it takes to perform each full-wave field calculation. However, with the advances in computing speed, and the onset of parallel processing, this practical consideration will likely be overcome.

The feasibility of the method on matched field inversion problems was demonstrated by several inversions of a synthetic environment. The environment consisted of a shallow water wave guide overlying an ocean bottom consisting of homogeneous elastic solid layers. The acoustic field produced by a shallow acoustic source was sampled at close range by a vertical line array. The first inversion example demonstrated the performance of the

method under optimum conditions, a noise-free environment and absolute certainty in the source/array geometry.

The inversion of the synthetic environment, even under idealized conditions, illustrated the formidable task of estimating the globally optimum parameter configuration caused by the complexity of the parameter space. The parameter space is replete with local optima caused by the inter-relationships of the geoacoustic parameters, and the richly multipath environment, which is sensitive to slight changes in the geoacoustic properties of the ocean wave guide.

Despite the difficulty of the problem, the inversion method was very successful in estimating the values of the geoacoustic parameters. Estimates lay between 1% and 15% of their actual values within their assigned ranges, for sensitive and insensitive parameters respectively.

Two examples were presented in order to demonstrate the performance of the inversion method when there is an uncertainty in the assumed source/array geometry, a common situation in field experiments. The inversion method was successful in estimating the values of the geoacoustic parameters, although less successful than in the case with absolute geometric certainty. The estimates of the sensitive parameters remained relatively accurate. The less sensitive parameters, however, were moderately accurate.

The degradation in the parameter estimates results from the dependence of the inversion method on accurate modeling of the wave field. The introduction of an error in the source/array geometry is equivalent to subtly altering the wave field at the array. Larger errors in the source/array geometry lead to increasing degradation of the parameter estimates.

Two examples were presented in order to demonstrate the performance of the inversion method when there is noise contamination, a situation arising in all field experiments. Signal-to-noise ratios representing realistic noise contamination and a high degree of noise contamination were considered.

Noise alters the pressures at the hydrophone array. The error is similar to that incurred with an erroneous source/array geometry, only to a more marked degree, and randomly rather than coherently. The inversion method attempts to reproduce the perturbed pressures, and therefore has difficulty estimating the geoacoustic parameters. The method performs relatively well under a realistic level of background noise, but degrades almost to the point of inutility under extreme noise.

The simulation examples showed that the accuracy of the wave field modeling, while providing much of the power of the inversion method, is also an inherent weakness. However, reasonable parameter estimates are obtained for moderate uncertainty in the source range and realistic background noise.

The utility of the inversion method was demonstrated on acoustic field data collected in an experiment conducted in shallow water, overlying a thick layer of unconsolidated sediments and sedimentary bedrock. The acoustic field produced by a shallow acoustic source was sampled by a vertical line array of 10 hydrophones at a distance of approximately 1.5 km.

The inversion of the geoacoustic properties of the sea floor at the experimental site was a success. The parameters converged within expected ranges, and produced a reasonable, and mutually consistent set of parameter values. The associated replica acoustic field correlated very highly with the measured field, to approximately 0.975.

The success of the inversion on acoustic field data, obtained with modest uncertainty in the source/array geometry, noise contamination and mismatch between the simplified model and the environment, attests to the robustness of the self-guided, randomized search method, coupled to the precision of the matched field method and the acoustic propagation model.

B. Suggestions for Further Research

Suggestions for future research essentially fall into two categories: validation studies involving other experiments, and the application of the generalized inversion method to problems from different disciplines.

In order to overcome the dependence of the inversion method on the accuracy of the wave field sampled at the hydrophone array, a study of the effect of increasing the effective array aperture should be performed. It may be postulated that correlating replica acoustic fields with data measured at arrays separated by several wavelengths would reduce susceptibility to noise and geometric uncertainty. Equivalently, and more cost effectively, the acoustic field generated by acoustic sources at incremental ranges could be replicated. The SAFARI program (Schmidt, 1990) takes the same amount of time to compute the acoustic field at multiple ranges.

For existing field data, the replica acoustic data could be computed at several frequencies. It may be postulated that performing the inversion at multiple frequencies would reduce the susceptibility to noise. It is also possible that performing the inversion at several discrete frequencies would be more effective than frequency averaging.

It would also be informative to perform a more exhaustive study of model mismatch to the environment. This must be performed using more realistic models, perhaps taking into account range dependence, scattering, and layering. Though the results would be problem specific, it may be possible to determine which simplifications are unacceptable, as might be the assumption of range-independence in a range-dependent environment.

It would be instructional to examine the cross-correlation of the geoacoustic parameters. Accounting for parameter cross-correlation in this manner would reduce the error incurred by considering each parameter separately. The information could be used to guide the search through the parameter space more efficiently. If parameter variations correlate strongly

B. Suggestions for Further Research

Suggestions for future research essentially fall into two categories: validation studies involving other experiments, and the application of the generalized inversion method to problems from different disciplines.

In order to overcome the dependence of the inversion method on the accuracy of the wave field sampled at the hydrophone array, a study of the effect of increasing the effective array aperture should be performed. It may be postulated that correlating replica acoustic fields with data measured at arrays separated by several wavelengths would reduce susceptibility to noise and geometric uncertainty. Equivalently, and more cost effectively, the acoustic field generated by acoustic sources at incremental ranges could be replicated. The SAFARI program (Schmidt, 1990) takes the same amount of time to compute the acoustic field at multiple ranges.

For existing field data, the replica acoustic data could be computed at several frequencies. It may be postulated that performing the inversion at multiple frequencies would reduce the susceptibility to noise. It is also possible that performing the inversion at several discrete frequencies would be more effective than frequency averaging.

It would also be informative to perform a more exhaustive study of model mismatch to the environment. This must be performed using more realistic models, perhaps taking into account range dependence, scattering, and layering. Though the results would be problem specific, it may be possible to determine which simplifications are unacceptable, as might be the assumption of range-independence in a range-dependent environment.

It would be instructional to examine the cross-correlation of the geoacoustic parameters. Accounting for parameter cross-correlation in this manner would reduce the error incurred by considering each parameter separately. The information could be used to guide the search through the parameter space more efficiently. If parameter variations correlate strongly

to variations in other parameters, the parameters could be perturbed in tandem in order to reduce the number of unrealistic configurations examined. This could be implemented as a weighting function to the probability distributions from which the parameter perturbation values are determined.

It would also be worth examining the effects of a time-varying solution. This would be relatively straightforward to implement as a simulation. This information would determine the utility of the technique as a real-time inversion method. If successful, the method could be used as either an operational survey technique, or as a feedback routine imbedded in a source localization routine.

The black box nature of inversion method allows it be generalized to any optimization problem that can be cast such that a cost function yields a scalar output representing the validity of a configuration of discrete parameters in replicating a desired condition. It would be useful to determine the utility of the inversion method on non-related data sets. It would probably do very well on data sets in which the forward modeling time is relatively small.

In conclusion, the method developed in this thesis was successfully applied to a matched field inversion problem, and has several advantages over conventional techniques that make it promising as an optimization technique for inversion problems from other disciplines.

References

Basu, A., and Fraser, N.
Rapid determination of the critical temperature in simulated annealing inversion, Journal of Science, Vol. 249, p. 1409-1412, 1990.

Bornhold, B.D., and Yorath, C.J.
Surficial geology of the continental shelf, northwestern Vancouver Island , Marine Geology, Vol. 57, p. 89-112, 1984.

Carter, L.
An evaluation of the provenance of terrigeneous sediments from offshore Vancouver Island , Canadian Journal of Earth Science, Vol. 11, p. 664-677, 1973.

Surficial sediments of Barkley Sound and adjacent continental shelf, west coast Vancouver Island, Canadian Journal of Earth Science, Vol. 10, p. 441-459, 1973.

Chapman, N.R.
Source levels of shallow explosive charges, Journal of the Acoustical Society of America, Vol. 84, p. 679-702, 1988.

Energy, Mines and Resources.
Chart of the shelf region off southern Vancouver Island, 1990.

Fizell, R.G.
Application of high resolution processing to range and depth estimation using ambiguity function methods, Journal of the Acoustical Society of America, Vol. 86, p. 606-613, 1987.

Gill, A.E.
Atmosphere-Ocean Dynamics, International Geophysics Series, Vol. 30, 1982.

Gingras, D.F.
Methods for predicting the sensitivity of matched field processors to mismatch, Journal of the Acoustical Society of America, Vol. 86, p. 1940-1949, 1989.

Hamilton, E.L.
Acoustic Properties of Sediments, Acoustics and Ocean Bottom, II FASE Conference, Madrid, p.3-58, 1987.

Geoacoustic Modeling of the Sea Floor, Journal of the Acoustical Society of America, Vol. 68, p. 1313-1340, 1980.

Prediction of in situ acoustic and elastic properties of marine sediments, Geophysics, Vol. 36, p. 266, 1971.

Shear wave velocity versus depth in marine sediments: a review, Geophysics, Vol. 41, p. 985, 1976.

Sound Velocity-Density Relations in Sea Floor Sediments and Rocks, Journal of the Acoustical Society of America, Vol. 63, p. 366-377, 1977.

Vp/Vs and Poisson's Ratios in Marine Sediments and Rocks, Journal of the Acoustical Society of America, Vol. 66, p. 1093-1101, 1979.

Harrison, C.H. and Cousins, P.L.
A Study of Propagation Loss Dependence on Sediment Layer Thickness Using the Fast Field Program, In Ocean Seismo-Acoustics: Low Frequency Underwater Acoustics, Ed. T. Akal and L.M. Berkson, NATO Conference Series Vol(16), Plennium Press, 1986.

Herzer, R.H., and Bornhold, B.D.
Glaciation and Post-Glacial History of the Continental Shelf Off Southwestern Vancouver Island, British Columbia, Marine Geology, Vol. 48, p. 285-319, 1982.

Kirkpatrick ,S., Gelatt, C.D. and Vecchi, M.
Optimization by Simulated Annealing, Journal of the Science, Vol. 220, p. 671-680, 1983.

Kirkpatrick, S.
Optimization by Simulated Annealing, Journal of the Statistical Physics Vol. 34, p. 975-986, 1984.

Luternauer, J.L., Murray, J.W.
Late Quarternary morphological development and sedimentation, central British Columbia Continental Shelf , Geological Survey of Canada paper 83-12, 1983.

Meisenner, R.
P- and Sv- wave from uphole shooting, Geophysical Prospecting, Vol(13), p. 433, 1965.

Ohta, Y. and Goto, N.
Empirical shear wave velocity equations in terms of soil indexes, Earthquake Engineering and Structural Dynamics, Vol(6), p. 167, 1978.

Press, W.H., Flannery, B.P., Teukolsky, S.A. and Vetterling, W.T.
Numerical Recipes in the Art of Scientific Computing, Cambridge University Press, New York, New York, 1986.

Scheuer, T., Pettigrew, R. and Horwitz, A.
A Study of Matched Field Processing Technology, Macdonald Dettwiler, Contractor's Report (Defence Research Establishment Pacific), March 1991.

Schmidt. M.
SAFARI user's guide, Contractor's Report, Defence Research Establishment Pacific, 1990.

Sen, M.K., and Stoffa, P.L.
Nonlinear one-dimensional seismic waveform inversion using simulated annealing, Journal of Geophysics, Vol. 56, No. 10, p. 1624-1638, 1991.

Shouldice, D.H.
Western Canadian Continental Shelf, in R.G. McGrossan, ed., Future Petroleum Provinces of Canada: Canadian Society of Petroleum Geologists Memoir 1, p. 7-35, 1973.

Smith, D.T.
Geotechnical Characteristics of the Sea Bed Related to Seismo-Acoustics, In Ocean Seismo-Acoustics: Low Frequency Underwater Acoustics, Ed. T. Akal and L.M. Berkson, NATO Conference Series Vol(16), Plennium Press, 1986.

Stoll, R.D.
Acoustic Waves in Marine Sediments, In Ocean Seismo-Acoustics: Low Frequency Underwater Acoustics, Ed. T. Akal and L.M. Berkson, NATO Conference Series Vol(16), Plennium Press, 1986.

Tiffin, D.L., Cameron, B.E.B. and Murray, J.W.
Tectonic and Depositional History of the Continental Margin off Vancouver Island, British Columbia, Canadian Journal of Earth Sciences, Vol. 9, p. 280-296, 1972.

Tolstoy, A.
Sensitivity of matched field processing to sound speed profile mismatch for vertical arrays in a deep water Pacific environment, Journal of the Acoustical Society of America, Vol. 85, p. 2394-2404, 1989.

van Laarhoven, P.J.M., and Arts, E.H.L.
Simulated Annealing: Theory and Applications, Reidel, Dordretch, 1987.

Weinberg, H.
Generic Sonar Model, Naval Underwater Systems Center Technical Document 5971D, 6 June 1985.

Zeller, R.M.
The seasonal and inter-annual variability of the ocean features at the enterance to Juan de Fuca Strait. Unpublished MSc Thesis, Royal Roads Military College, Vict., B.C., 1990.

VITA

Colin Edwards Lindsay

Born 14 February 1969 at San Francisco, California

Educational Institutions Attended:

Royal Roads Military College	1986 to 1990
University of Victoria	1990 to 1992

Degrees Awarded:

B.Sc. (Honours)	Royal Roads Military College`	1990

Honours and Awards:

Lieutenant Governor General's Silver Medal	1989
Governor General's Silver Medal	1990
NSERC Science Scholarship	1990-92
President's Award Scholarship	1990-92

PARTIAL COPYRIGHT LICENSE

I hereby grant the right to lend my thesis (the title of which is shown below) to users of the University Library, and to make single copies only for such users or in response to a request from the library or any other university, or similar institution, on its behalf or for any of its users. I further agree that permission for extensive copying of this thesis for scholarly purposes may be granted by me or a member of the university designated by me. It is understood that copying or publication of this thesis for financial gain shall not be allowed without my written permission.

Title of Thesis:

MATCHED FIELD INVERSION
OF GEOACOUSTIC MODEL PARAMETERS
USING ADAPTIVE SIMULATED ANNEALING

Author [redacted]

Signature

Colin Edwards Lindsay

11 Dec 92

Date